Defense Nuclear Agency
Alexandria, VA 22310-3398

DNA-TR-95-88

Improved Threat Correlation from Higher Fidelity X-Ray Sources on SATURN

Dr. Phillip Greene
Science Research Lab
15 Ward Street
Somerville, MA 02143

November 1996

Technical Report

CONTRACT No. DNA 001-92-C-0104

DISCLAIMER

"The views and conclusions contained in this document are those of the author and should not be interpreted as representing the official policies, expressed or implied, of the U.S. Government."

DESTRUCTION NOTICE:

Destroy this report when it is no longer needed.
Do not return to sender.

PLEASE NOTIFY THE DEFENSE SPECIAL WEAPONS AGENCY, ATTN: CSTI, 6801TELEGRAPH ROAD, ALEXANDRIA, VA 22310-3398, IF YOUR ADDRESS IS INCORRECT, IF YOU WISH IT DELETED FROM THE DISTRIBUTION LIST, OR IF THE ADDRESSEE IS NO LONGER EMPLOYED BY YOUR ORGANIZATION.

DISCLAIMER NOTICE

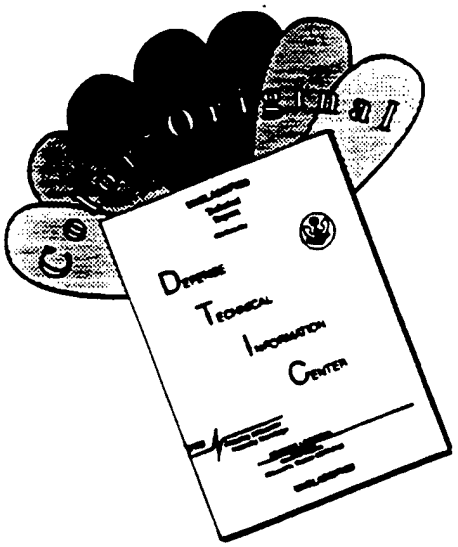

THIS DOCUMENT IS BEST QUALITY AVAILABLE. THE COPY FURNISHED TO DTIC CONTAINED A SIGNIFICANT NUMBER OF COLOR PAGES WHICH DO NOT REPRODUCE LEGIBLY ON BLACK AND WHITE MICROFICHE.

DISTRIBUTION LIST UPDATE

This mailer is provided to enable DSWA to maintain current distribution lists for reports. (We would appreciate your providing the requested information.)

NOTE:
Please return the mailing label from the document so that any additions, changes, corrections or deletions can be made easily. For distribution cancellation or more information call DSWA/IMAS (703) 325-1036.

☐ Add the individual listed to your distribution list.

☐ Delete the cited organization/individual.

☐ Change of address.

NAME: _____

ORGANIZATION: _____

OLD ADDRESS	CURRENT ADDRESS
_____	_____
_____	_____
_____	_____

TELEPHONE NUMBER: ( ) _____

DSWA PUBLICATION NUMBER/TITLE	CHANGES/DELETIONS/ADDITIONS, etc.) *(Attach Sheet if more Space is Required)*
_____	_____
_____	_____
_____	_____

DSWA OR OTHER GOVERNMENT CONTRACT NUMBER: _____

CERTIFICATION OF NEED-TO-KNOW BY GOVERNMENT SPONSOR (if other than DSWA):

SPONSORING ORGANIZATION: _____

CONTRACTING OFFICER OR REPRESENTATIVE: _____

SIGNATURE: _____

CUT HERE AND RETURN

DEFENSE SPECIAL WEAPONS AGENCY
ATTN: IMAS
6801 TELEGRAPH ROAD
ALEXANDRIA, VA 22310-3398

DEFENSE SPECIAL WEAPONS AGENCY
ATTN: IMAS
6801 TELEGRAPH ROAD
ALEXANDRIA, VA 22310-3398

REPORT DOCUMENTATION PAGE

Form Approved
OMB No. 0704-0188

1. AGENCY USE ONLY (Leave blank)	2. REPORT DATE	3. REPORT TYPE AND DATES COVERED
	961101	Technical 920929 - 950328

4. TITLE AND SUBTITLE
Improved Threat Correlation from Higher Fidelity X-Ray Sources on SATURN

5. FUNDING NUMBERS
C - DNA 001-92-C-0104
PE - 62715H
PR - A, A
TA - A, A
WU - DH325740

6. AUTHOR(S)
Dr. Phillip Greene

7. PERFORMING ORGANIZATION NAME(S) AND ADDRESS(ES)
Science Research Lab
15 Ward Street
Somerville, MA 02143

8. PERFORMING ORGANIZATION REPORT NUMBER
SRL-16-F-1995

9. SPONSORING/MONITORING AGENCY NAME(S) AND ADDRESS(ES)
Defense Special Weapons Agency
6801 Telegraph Road
Alexandria, VA 22310-3398
TDSP/Rowley

10. SPONSORING/MONITORING AGENCY REPORT NUMBER
DNA-TR-95-88

11. SUPPLEMENTARY NOTES
This work was sponsored by the Defense Special Weapons Agency under RDT&E RMC Codes B4662D A A 00025 3100A 24904D and B4662D A A 00024 3100A 25904D.

12a. DISTRIBUTION/AVAILABILITY STATEMENT
Approved for public release; distribution is unlimited.

12b. DISTRIBUTION CODE

13. ABSTRACT (*Maximum 200 words*)

A summary of the development of a Metal Plasma Source (MPS) with proposed applications as the imploding PRS load on a high current z-pinch is presented. The load design is comprised of an array of Metal Vapor Vacuum Arc (MEVVA) sources which produce high density (~5 x 10^{16} ions/cm^3) titanium plasmas as demonstrated by two independent diagnostics. The MEVVA array, which has much greater azimuthal uniformity than a wire array of comparable diameter, delivers an annular load with selectable total mass and average diameter over of useful range of values. Also presented is a design for a novel Nested Shell load which utilizes the MPS as the inner shell. This Nested Shell has the possibility of leading to higher density, higher temperature pinches than are presently achieved with standard loads.

14. SUBJECT TERMS		15. NUMBER OF PAGES
Metal Plasma Source	Nested Shell Load	62
Metal Vapor Vacuum Arc	High Current Z-Pinch	16. PRICE CODE

17. SECURITY CLASSIFICATION OF REPORT	18. SECURITY CLASSIFICATION OF THIS PAGE	19. SECURITY CLASSIFICATION OF ABSTRACT	20. LIMITATION OF ABSTRACT
UNCLASSIFIED	UNCLASSIFIED	UNCLASSIFIED	SAR

NSN 7540-280-5500

Standard Form 298 (Rev.2-89)
Prescribed by ANSI Sts. 239-18
298-102

CLASSIFIED BY:

N/A since Unclassified.

DECLASSIFY ON:

N/A since Unclassified.

CONVERSION TABLE

Conversion factors for U.S. Customary to metric (SI) units of measurement

MULTIPLY → BY → TO GET
TO GET ← BY ← DIVIDE

angstrom	1.000 000	XE -10	meters (m)
calorie (thermochemical)	4.184 000		joule (J)
cal (thermochemical)/cm^2	4.184 000	XE -2	mega joule/m^2 (MJ/m^2)
degree (angle)	1.745 329	XE -2	radian (rad)
degree Fahrenheit	$T_K = (T\ °F + 459.67)/1.8$		degree kelvin (K)
electron volt	1.602 19X E -19		joule (J)
inch	2.540 000	XE -2	meter (m)
micron	1.000 000	XE -6	meter (m)
torr (mm Hg, 0° C)	1.333 22XE -1		kilo pascal (kPa)

TABLE OF CONTENTS

FIGURES

FIGURES (Continued)

SECTION 1

INTRODUCTION

This document is the Final Report for DNA contract DNA001-92-C-0104 "Improved Threat Correlation From Higher Fidelity X-Ray Sources on SATURN". It summarizes the work performed under this contract in the development of the Metal Plasma Source for the period September 1992 - April 1995. Experiments were performed on a test stand at Science Research Laboratory to confirm the capabilities of the Metal Plasma Source. This document will describe the planned tests, and the accomplishments of Science Research Laboratory in the development of the source for the proposed tests.

In this project Science Research Laboratory (SRL) has developed a new type of imploding plasma x-ray source, called the Metal Plasma Source (MPS), consisting of an annular array of metal vapor vacuum arc (MEVVA) sources which deliver a highly collimated, azimuthally uniform plasma shell. Present standard imploding loads consisting of either wire arrays or supersonic gas puffs are not ideal imploding loads. Wire arrays start off with an initial azimuthal asymmetry which may lead to increased growth of instabilities during the implosion, and hence limit the compression ratio and ultimate x-ray yield. Gas puffs are not initially well ionized. This poor initial ionization may lead to a non-uniform current sheet, or may not implode all of the mass. Although improvements have been made to gas puffs by tilting nozzles and better pre-ionization, and the higher current simulators such as JUPITER may use thin foils instead of wires, the development of a more nearly ideal load is important for increasing x-ray yield from today's simulators, as well as for proper scaling and design for future simulators. The MPS, which has a high

degree of ionization, approaches the ideal shell for an imploding load. The initial azimuthal asymmetries of the MPS may be drastically reduced over wire arrays at comparable radii. The mass delivered by the MPS can be "tuned" to different values, and different azimuthal distributions that are not achievable with wire arrays. Since the MPS starts off as a plasma with a fractional ionization approaching unity, the issue of pre-ionization, which is felt to be important for gas puffs, is not of concern. In addition, due to the high initial ionization of the MPS, improved radial confinement above that of a gas puff may be achieved with an applied axial magnetic field. This field may also help reduce the growth of instabilities such as Raleigh-Taylor during the run-in phase of the implosion. This more ideal load may increase the compression ratio achieved, and increase the x-ray output. The predicted x-ray yield from PRS loads on future, higher current simulators such as DECADE, show that the ability to implode large radius loads greatly enhances the x-ray yield.[1] One key factor to the stable implosion of a large radius load is the initial uniformity of the load. As the radius increases, and the subsequent implosion time increases, instabilities have more time to exacerbate any initial non-uniformity. The MPS may allow the study of larger radius implosions than are feasible with wire arrays or gas puffs on today's simulators.

In addition to the single shell MPS, SRL has also designed another innovative source called the nested shell z-pinch, consisting of an outer, low atomic number shell, such as CH_4, driven onto an inner, high atomic number shell, such as Ti, Cu, Kr, Mo or Nb. The nested shell is a radically new load configuration for high current simulators. The outer shell carries the current initially, shunting current only late in the current rise-

time to the inner shell, as the outer shell stagnates on the inner. Thus the outer shell acts like a pulse-sharpening switch, effectively sharpening the simulator drive current pulse seen by the inner shell. The sharpened current pulse reduces the time for detrimental instabilities, such as Raleigh-Taylor, to develop. With such a transformed current drive, the inner shell may implode to the axis in a more stable manner, form a high density, higher temperature pinch, and produce K-shell x-rays with higher efficiency than is presently achieved with the standard single shell implosion.

Today's high current simulators exhibit a precipitous drop in K-shell conversion efficiency as the atomic number of the load is increased. For example, SATURN produces 40 kJ of Ar x-rays (3.2-4 keV), decreasing to 10 kJ of Ti (4.7-5.0 keV) and only 2 kJ of Cu (8-10 keV). The total x-ray output is ~500 kJ in all cases, showing that the standard single shell implosions used today are very inefficient at converting the reservoir of energy into K-shell x-rays. The high degree of initial non-uniformities of standard loads may be an important factor limiting the efficiency. Computer models with ideal loads show much higher compression ratios, and correspondingly higher yields than are achieved with gas puffs and wire arrays. The use of the more ideal MPS may narrow the gap between the predicted and measured yields. If the nested shell configuration can be effectively used to sharpen the simulator current pulse to the inner shell, simple estimates suggest that the nested shells proposed here might increase the K-shell yields from Cu to 10-20 kJ, for the same ~10 MA SATURN current. With the novel source being developed by SRL, other elements such as Kr, Mo and Nb might achieve the efficiencies of lower atomic number elements. The low masses of the nested shell loads, as well as requirements for high

azimuthal uniformity and initial ionization, require the development of the MPS for the nested shell loads. If these dramatic improvements over today's yields are realized, this type of implosion on SATURN would offer ~0.5-1.0 cal/cm^2 fluences of 8-20 keV x-rays to test objects behind survivable debris shields. At present, the bremmstrahlung environments are still able to deliver only >15-20 keV hot x-rays for electromagnetic effects testing. This novel load has the potential to significantly enhance the fidelity of aboveground effects tests, particularly for spot shielded circuits, but more generally to improve AGT/UGT and Threat Correlation.

1.1 STATEMENT OF WORK (SOW).

The work sponsored under this contract is broken down into three main tasks. A summary of the original SOW for these tasks is presented below.

TASK 3.1 Analyze Demonstration Test of Nested Shell Concept.

The contractor shall analyze the results of demonstration tests of nested shell loads as identified in Reference 2. The focus of this analysis shall be oriented toward development of conceptual designs for better collimated gas jets for use as outer and/or inner drivers for z-pinches.

TASK 3.2 Develop a Prototype Metal Plasma Source For Use In An Imploding Plasma Test Bed.

The contractor shall design, fabricate, and test a metal plasma source for application as the plasma source in an imploding plasma (z-pinch) test-bed. This source

shall be capable of producing Cu or Ti plasmas whose spatial and temporal distributions shall be measured. These metal plasma sources shall be designed in a manner allowing for fielding on different potential SNL or DNA x-ray simulators with only minor hardware modifications required. The plasma source fabricated shall be tested and characterized on the bench at Science Research Laboratory (SRL) prior to shipment to a high current x-ray simulator facility. The plasma source will then be utilized to demonstrate a higher efficiency single shell z-pinch implosion on the simulator during two, two week experiments.

TASK 3.3 Optimization of Nested Shell Implosions On SATURN.

The contractor shall work in coordination with the staff at a high current simulator facility to design, develop, fabricate, and test nested shell loads utilizing either a Cu or Ti plasma for the inner shell, and a lower Z material, such as a Carbon plasma or CH_4 gas puff, as the outer shell. These tests shall be conducted during two, two week pulsings. Adequate diagnostics shall be fielded during these tests to allow for measurement of the K-shell yield from the nested shell implosion, the full time history of the radiation pulse generated, and digital imaging data of the implosion process. These data shall be used to optimize the design of nested shell sources for SATURN and DNA x-ray simulators.

1.2 WORK BREAKDOWN STRUCTURE (WBS).

In the following Work Breakdown Structure (WBS), SRL's course of action for accomplishing the tasks in the SOW are presented. At a global level the WBS reflects the four major tasks of the SOW. The reason for the breakdown structure for Task 3.1 is

readily apparent. The logic behind the organization of Tasks 3.2 and 3.3 is described below.

Table 1-1. Improved threat correlation from higher fidelity x-ray sources.

3.1	**Analyze Demonstration Test of Nested Shell Concept** 3.1.1 Analyze Test of Nested Shell Concept with Wires on Gas Puff 3.1.2 Conceptual Design of Better Super-Sonic Gas Puffs
3.2	**Develop Prototype Metal Plasma Source (MPS)** ***Mark-I*** 3.2.1 Develop Single Shell of Ti 3.2.1.1 Design, Fabricate and Assemble Single Shell Test Bed 3.2.1.2 Bench Test Single Diode of Ti ***Mark-II*** 3.2.1.3 Upgrade to N Diode Single Shell of Ti 3.2.1.4 Bench Test Single Shell of Ti 3.2.2 Integrate Single Ti Shell into SATURN 3.2.3 Test Single Shell Implosions on SATURN
3.3	**Optimization of Nested Shell Implosions on SATURN** 3.3.1 Develop Nested Shell of C/Ti 3.3.1.1 Design, Fabricate and Assemble Outer Driver Shell 3.3.1.2 Bench Test Outer Driver Shell 3.3.1.3 Bench Test Nested Shell 3.3.2 Integrate Nested Shell into SATURN 3.3.3 Test Nested Shell on SATURN

365bc001

The primary challenge associated with creating this new metal plasma source for PRS applications is generating a highly collimated plasma of sufficient density and mass. To maximize x-ray yield, the load plasma must start at the proper annular radius, with the proper total mass required to ensure that the plasma implodes near the peak of the driver current. In addition, the kinetic energy of the ions must be greater than the K-shell excitation energy. This implies optimizing the radial mass distribution to give the optimum radial run-in velocity. For Ti implosions on Double Eagle, a possible configuration is an

annulus with an ID of 1 cm, and an OD of 5 cm. A simple model of the implosion predicts that the mass per unit length required for that configuration to implode just after the peak in the current pulse is 55 μg/cm. For Ti, this implies an ion density of ~3.7×10^{16} cm^{-3}. For the SATURN driver, the necessary mass is greater, and hence the ion density required for those same initial dimensions would be ~5×10^{16} cm^{-3}. Other configurations with both higher and lower densities are of course possible. Since densities this large had not yet been measured from a MEVVA-type discharge, SRL decided that it would be prudent to develop this task with a two-phase, Mark-I/Mark-II progression, with the Mark-I test-bed much smaller than the final hardware. The Mark-I apparatus would allow validation of the density capabilities of the MPS, before committing to the major hardware needed in Mark-II. The goal of the Mark-I assembly and test phase is to refine the design parameters for the larger Mark-II MPS apparatus.

Task 3.2 Develop a Prototype Metal Plasma Source

The MPS consists of an annulus of 10-30 MEVVA diodes of Ti. Plasmas are drawn from these MEVVA diodes and then guided into the z-pinch diode region. Each of the sub-tasks of the prototype MPS development is now discussed briefly.

3.2.1 Develop a single shell of Ti

Mark-I Phase

3.2.1.1 Design, fabricate and assemble a single MEVVA diode test-bed

A single MEVVA diode test-bed will be designed and assembled. This test-bed will be used to study the source density from the diode and the behavior of the plasma in the magnetic field.

3.2.1.2 Bench test single MEVVA diode of Ti

Successful completion of the above is to validate the MEVVA/MPS approach, and set the guidelines for the Mark-II upgrade.

Mark-II Phase

3.2.1.3 Upgrade to N diode single shell of Ti

The Mark-II hardware is to be fabricated and assembled according to the guidelines set by the Mark-I device. A complete annular shell of Ti diodes in vacuum hardware compatible with the simulator facility is to be readied for testing.

3.2.1.4 Bench test single shell of Ti

Tests will be performed at SRL to characterize the azimuthal uniformity, the scaling of density with the number of diodes N, and the mass per unit length loading.

3.2.2 Integrate single shell Ti shell into x-ray simulator facility

Ensure that the Mark-II hardware is completely compatible with the simulator facility hardware, make any necessary adjustments, and confirm that the MPS operates reliably in the simulator environment.

3.2.3 Test single shell implosions

The proposed tests were two, 2 week testings to optimize the single shell implosions.

Task 3.3 Optimization of Nested Shell Implosions on SATURN

This task is to develop a nested shell MPS.

3.3.1 Develop Nested Shell of C/Ti

The plan is to develop an outer driver shell of CO_2 or CH_4 around the single shell MPS developed in task 3.2.

3.3.1.1 Design, fabricate and assemble outer driver shell

Based upon the experience with the single shell MPS, an outer driver shell of CO_2 or CH_4 will be designed.

3.3.1.2 Bench test outer driver shell

The outer shell will be tested for azimuthal uniformity, and to ensure the desired mass per unit length.

3.3.1.3 Bench test Nested Shell

The combined inner and outer shells will be tested to ensure synchronism of the two shells in the load region, separation of the shells and the proper mass loadings.

3.3.2 Integrate Nested Shell into simulator facility

Install the Nested Shell MPS apparatus in simulator.

3.3.3 Test Nested Shell on simulator

Two, 2 week pulsings were planned to test the Nested Shell MPS.

The remainder of this report is organized into the following sections:

- Section 2: Summary of Task 3.1
- Section 3: Summary of Task 3.2
- Section 4: Summary of Task 3.3
- Section 5: Conclusions
- Section 6: References

SECTION 2

SUMMARY OF TASK 3.1

Task 3.1 has been broken down into tasks Task 3.1.1, the analysis of the demonstration tests, and Task 3.1.2, the conceptual designs of better supersonic gas puffs. Designs and tests of improved supersonic nozzles which were under way at SRL under separate funding during the period of performance of this contract allowed synergy between these two projects. A summary of the nozzle design follows the summary of the results from the preliminary nested shell tests.

The preliminary test of the Nested Shell concept were CH fibers surrounding an Ar gas puff on the SATURN driver. The preliminary test of the nested shell concept has produced results that strongly motivate further development of the concept with a more ideal source such as the MPS. The nested shell was expected to:

(i) shunt the current from the outer pusher to the inner target shell

(ii) produce a faster and hence more stable pinch

(iii) produce a tighter and hence higher density pinch

(iv) produce a higher temperature pinch

All of the above should increase the conversion of available energy by the pinch into K-shell x-rays.

Despite the non-ideal nested geometry that was tested, the following results were obtained:

(i) the current was (at least) partially commutated from the outer to the inner shell, as shown by the streak images

(ii) the velocity of the inner Ar pinch at assembly (≈100 cm/ms) is higher than velocities inferred for the standard Ar gas puffs on SATURN earlier

(iv) the FWHMs of the x-ray pulses were the narrowest ever measured from high current simulators, either with wires or gas puffs. Although the total K-shell yield for these shots was lower than for standard puffs, the narrow widths made the K-shell power comparable to that from the standard shots. Such narrow widths might not be important for soft x-ray simulation fidelity, but they suggest ways to improve the black-body temperature of imploding shells for ICF research

(v) the compression ratio of the pinch (initial mean radius/final radius) was measured to be as high as 18:1, vs the typical 7:1 for standard gas puffs and wire arrays. The inductance of the pinch at maximum compression is therefore 5.8 nH/cm, vs the typical 3.9 nH/cm for the 7:1 compression. The higher pinch inductance allows more of the magnetic energy stored in the vacuum MITLs to be tapped by the pinch as well as enhancing the so called "anomalous" dissipation of magnetic energy.

(vi) unfortunately, the main failure of these exploratory nested shells is attributed to the lower density-temperature products that were inferred from the K-shell spectra as well

as the poor x-ray outputs. It is possible that this is due to the incomplete commutation of current from the outer CH fibers to the inner gas shell.

The nested shell concept was validated in part by the preliminary tests performed, and it may be inferred from the analysis of the results that the nested shell concept will be more efficient with closer to ideal geometries. The more ideal geometry may be from the MPS being developed in this project or from the improved gas puff nozzles which are discussed next.

New supersonic nozzle designs that emerged from this Task have already been applied to another DoD project. SRL has been funded by NSWC to develop and test improved supersonic nozzles for PHOENIX. These nozzles employ several features to make their configuration closer to ideal.

Shown in Figure 2-1 is a nozzle design which was characterized at SRL. The nozzle has an inward tilt to combat zippering. The nozzle also has a very narrow exit aperture (3 mm) to produce a thinner, hence closer to ideal, gas shell. The straight line contour design of the nozzle reduces manufacturing costs.

This nozzle design has been tested on the PHOENIX simulator, and for these tests, NRL's Plasma Radiation Branch performed numerical simulations of the implosion dynamics and K-shell radiation outputs. The inward tilt and narrow aperture have been found to be important for uniform assembly and maximum output. Utilizing this improved gas puff nozzle design, PHOENIX has been able to make significant progress towards

achieving useful amounts of Ar x-rays. With this nozzle design, approximately 20 kJ of Ar x-rays have been measured from a ~3.3 MA pinch on PHOENIX.

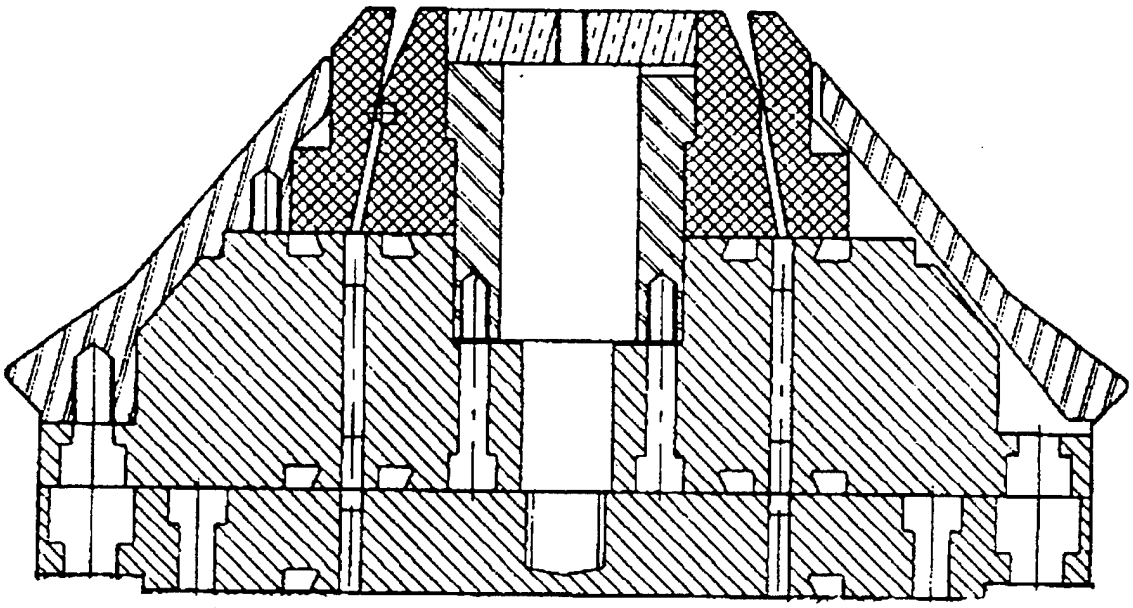

Figure 2-1. Improved gas puff nozzle design.

SECTION 3

SUMMARY OF TASK 3.2

3.1 DEVELOP A PROTOTYPE METAL PLASMA SOURCE.

The development of the prototype MPS has been the major push of this project. This type of source has clear advantages for both single and nested shell loads, if it can deliver adequate densities in the required distributions. However, inducing the MEVVA source to produce these densities, and fielding diagnostics which can unequivocally measure these densities of a metal plasma is non-trivial. Due to these difficulties, this portion of the project took more time than scheduled.

The initial Mark-I test-bed that was set-up at SRL is shown in Figure 3-1. The Mark-I apparatus was designed to be compatible with a wide range of cathode currents and magnetic field configurations and amplitudes. As will be described later in this section, there have been many changes made to the MEVVA capacitor circuit, and some changes in the trigger setup, but all the power supplies, and capacitors are still able to fit under a $9' \times 4'$ optical table.

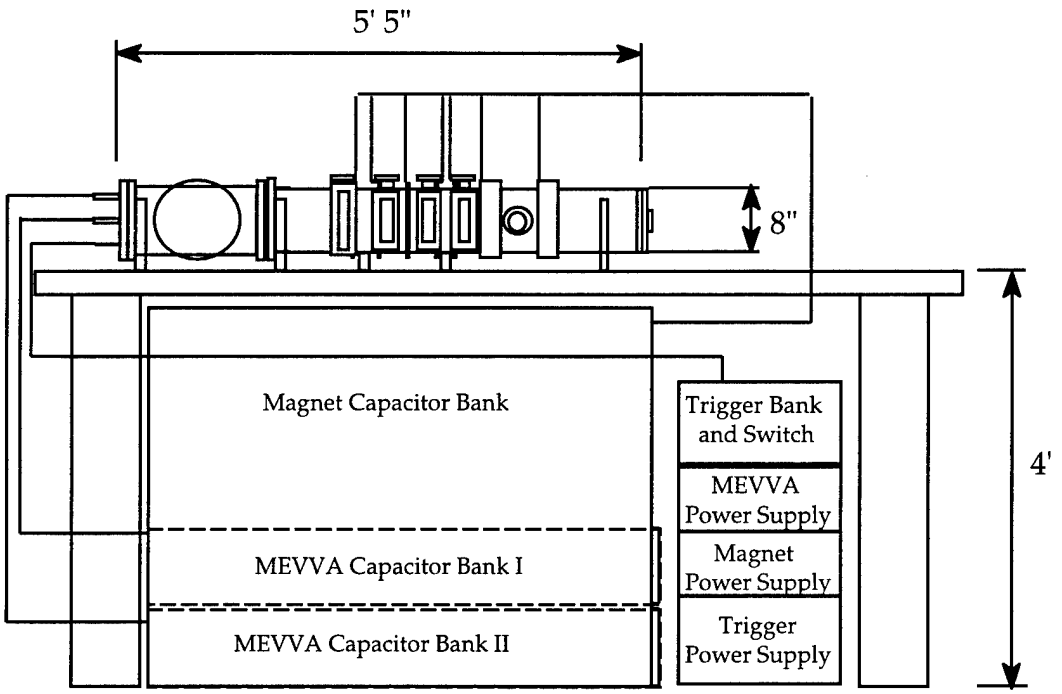

Figure 3-1. Overview of the Mark-I apparatus.

Due to an interest in the implosions of large diameter shells, the Mark-I apparatus has been designed to be able to test large diameter shell configurations as well as conventional size shells. The main vacuum chamber is constructed of an 8″ OD pipe with diagnostic access from 3 radial angles at four axial locations (Figure 3-2). The chamber has an inner diameter of 7.75″, and would allow testing of an annulus with a radius of up to about 7 cm.

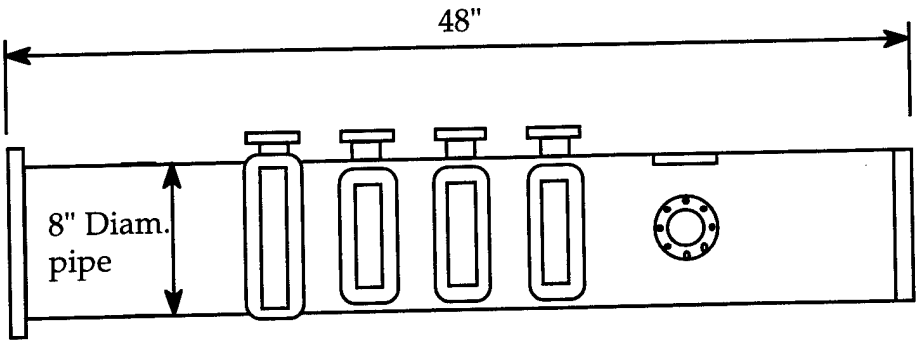

Figure 3-2. Mark-I main chamber.

The magnetic field coils and driver were designed to limit the required cost for the desired magnetic field. The coil for the magnetic field can be very easily modified. The coil can consist of a combination of two separate epoxy potted coils and coils of wire hand wound around the chamber. To minimize inductance, and hence driver cost, the coils are designed to fit directly onto the 8″ OD chamber. The driver circuit for the magnetic field consists of ~200 electrolytic capacitors, with a capacitance of 0.34 F at 700 volts, storing up to 83 kJ. The bank is switched by a 1 kV, high amperage SCR. To ensure that the circuit does not reverse and damage the capacitors, additional resistance in the form of a stainless steel resistor has been added to the circuit. The output of this circuit as a function of time with both the potted and hand wound coils at a charge voltage of 100 V is shown in Figure 3-3. The peak field on axis created by this coil configuration at 100 V is ~1700 G.

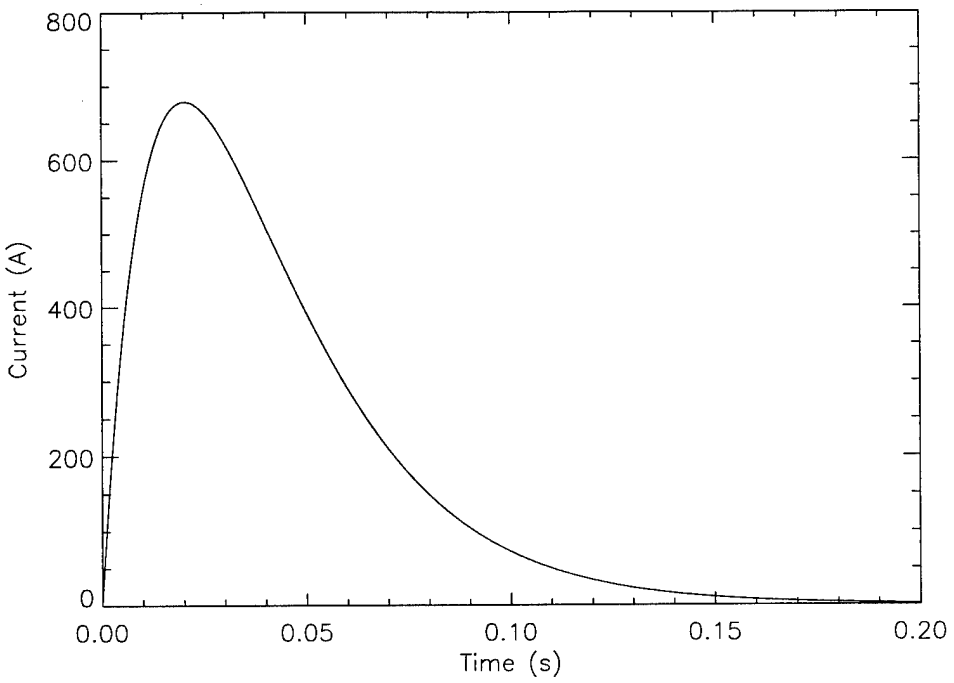

Figure 3-3. Current versus time for the Mark-I magnet bank.

This coil configuration was designed to test the confinement properties of the magnetic field, and to test the possibility of magnetically compressing the plasma in a converging field. Magnetic compression of the plasma was considered as an option to achieve the required plasma density at a cathode current density that did not greatly exceed previously achieved values.

The original designs of the MEVVA circuit, anode/cathode geometries, and feedthroughs were based upon the previous MEVVA work which was at lower current density. The cathode capacitor bank consisted of electrolytic capacitors in an E type LC ladder network. This type of ladder network can shape the output current to produce a

flat topped square wave. The designed pulse width was ~100 μs. The cathode feedthrough came in on the axis of the vacuum chamber, and made a radial step outward of about 6 cm. The displacement from the axis allowed measurements of the confinement of the plasma in a converging magnetic field. The anode was a double layer tungsten mesh, with a net transparency between 50 and 65%. The mesh was electrically connected to the vacuum chamber by a 1/4″ stainless steel plate attached to a section of stainless pipe which has Be-Cu fingerstock on its OD. The compressed fingerstock against the vacuum chamber wall completed the electrical contact to ground.

The initial design for triggering the discharge was a high voltage (≤20 kV) arc between tungsten trigger pins, and the cathode. The energy stored in the trigger circuit could be used to trigger more than one location on a diode, or more than one diode with a vacuum fan-out. This fan-out technique was brought to our attention by Dr. Mark Savage of SNL. Figure 3-4 shows a schematic of the trigger circuit. This triggering method readily lends itself to a fan-out, either just before the trigger pins, or with multiple capacitors, each individually firing trigger pins, but all switched with one spark gap. This second method is more likely to ensure an even distribution of the total energy in the trigger circuit. Although during the test on the Mark-I device we modified the triggering method to use a cable gun instead of a high voltage arc, the trigger circuit remains nearly identical, and still has the capability of the multiple fan-out.

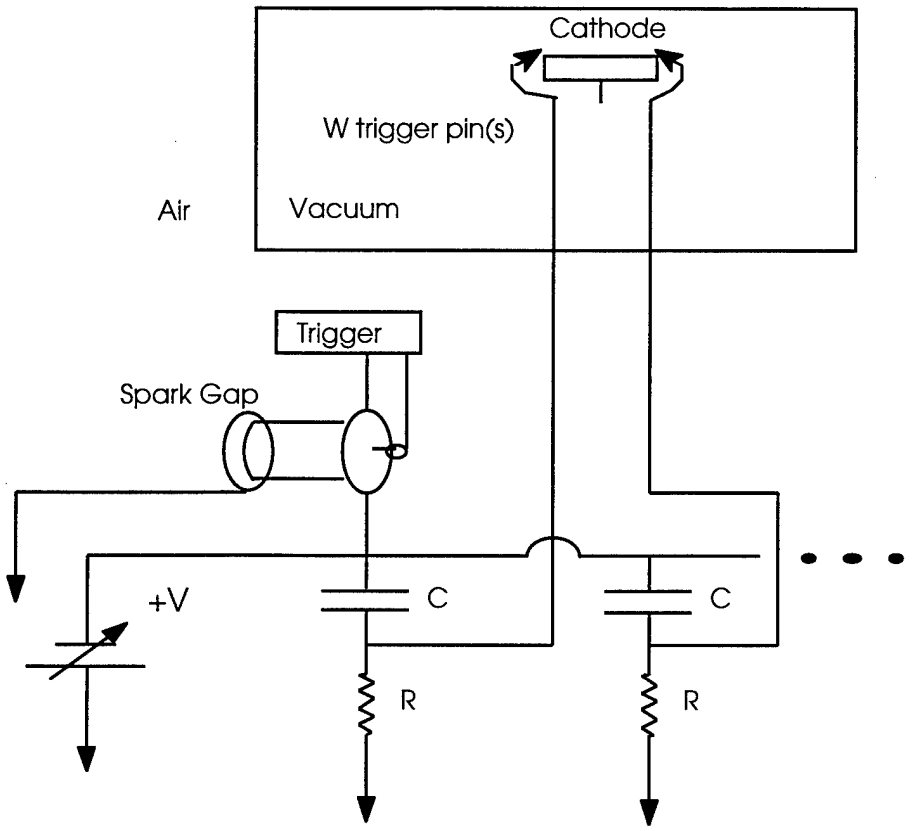

Figure 3-4. Trigger circuit.

The cable gun trigger has been found to be a more reliable trigger than the high voltage arc, and does not need to be as close to the MEVVA discharge. In addition, the cable gun trigger appears to initiate a more uniform discharge from the face of the cathode, probably because it is not as local a phenomenon as the high voltage arc. The cable gun used consists simply of a semi-rigid coaxial cable cut with a flat face, so it is inexpensive, and easy to replace.

Shown in Figure 3-5 is the typical MEVVA current pulse from the original Mark-I MEVVA bank at a charge voltage of -1000 V. The calculated pulse shape based upon the inductance of the leads, and the quoted inductance of the electrolytic capacitors is a square

wave of duration approximately 100 μs. However, for a short pulse duration such as this, the equivalent series resistance (ESR) of electrolytic capacitors is large, and the waveform does not match the anticipated shape, and the peak current is appreciably reduced. Unfortunately, the electrolytic capacitors which have been found to be very cost-effective for slower MEVVA circuits, are not as appropriate for use in this circuit.

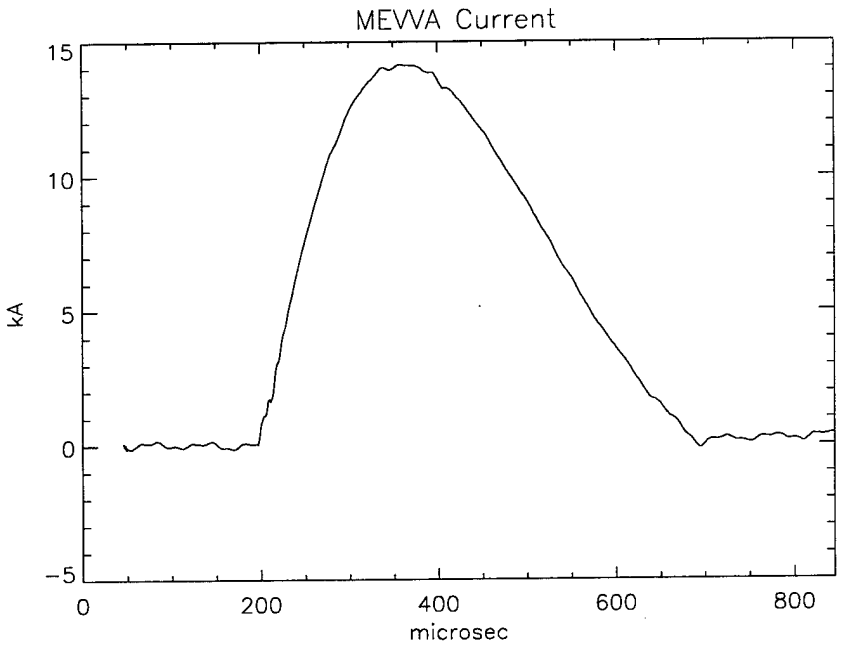

Figure 3-5. MEVVA current pulse at -1000 V charge with original, electrolytic capacitor bank.

In addition to the other diagnostics used, visible light emission from the plasma is a useful diagnostic for determining the spatial distribution of the plasma. The data presented here are open-shutter images of the plasma. This means that the light recorded is the time integrated light from all times during the discharge. It is exceedingly difficult to determine quantitatively a density from this type of data, so we do not attempt it. However, careful

corroboration of the visible light emissions from the plasma, and double probe measurements have shown that this diagnostic is remarkably good for determining the spatial extent of the plasma, and for qualitative information about the relative densities of various regions of the plasma.

The visible light emissions from the plasma have been used to demonstrate good radial confinement of a MEVVA plasma in a converging magnetic nozzle. The images are presented in Figure 3-6. The cathode was located off-axis in the chamber, and the expected trajectory of the plasma, if it strictly followed the field lines, is shown in Figure 3-7. These data were taken with cathode current densities of only 7 kA/cm^2, and have corresponding ion densities of only ~5×14 cm^{-3}, but they gave us strong hope that higher density plasmas could still be confined adequately, and possibly compressed to higher densities in static magnetic nozzles.

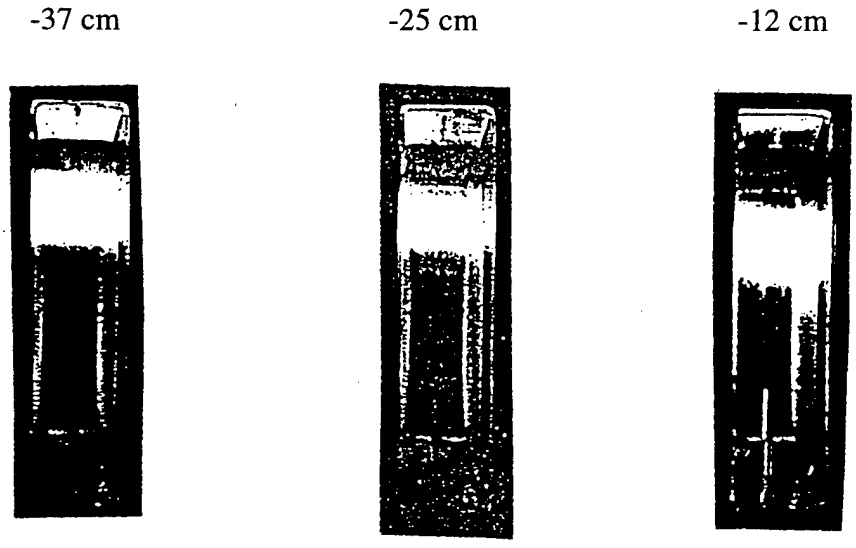

Figure 3-6. Light emitting region of the plasma at three locations.

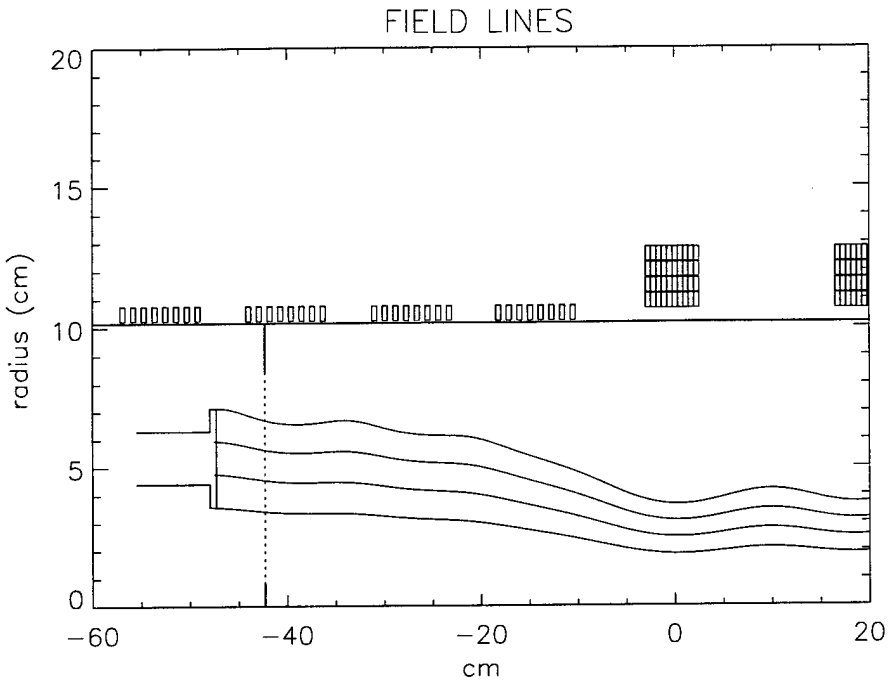

Figure 3-7. Trajectory of plasma strictly following flux tubes.

The electrolytic bank was used to investigate some of the confinement issues relevant to the project, but it was not capable of delivering the current needed to achieve the required density. Calculations performed by NumerEx for SNL[3] confirmed SRL's confinement studies at the densities achievable with this bank, but pointed out that the magnetic compression of the plasma would be limited. Hydrodynamic calculations performed by SRL have shown that magnetic compression of a plasma in a converging magnetic field is limited to less than a factor of two density increase.

The limit on the magnetic compression verifies that to achieve the densities estimated to be necessary for SATURN or another simulator, higher source densities are required. To push the MPS diodes to their maximum current and/or current density limits, the original low voltage, LC-ladder approach was abandoned in favor of a higher voltage,

faster capacitor network. To produce the desired peak current, capacitors were purchased to make a 3 kV, 1 mF, lower inductance bank. The electrical feed inside the vacuum was also changed to reduce the inductance. By shortening the overall path length in the vacuum, and by bringing the ground to a diameter of 1.5″, the inductance of this part of the circuit was reduced by a factor of four. A typical current trace of this circuit at a charge voltage of -1000 V is shown in Figure 3-8. Comparing this with the equivalent trace with the electrolytic bank (Figure 3-5), it can be seen that the reduced inductance and ESR has increased the peak current, and greatly shortened the pulse. This circuit can deliver a peak current over 100 kA into a single MPS diode, which should be contrasted with ~28 kA peak which was the maximum that could have been delivered by the older LC-ladder.

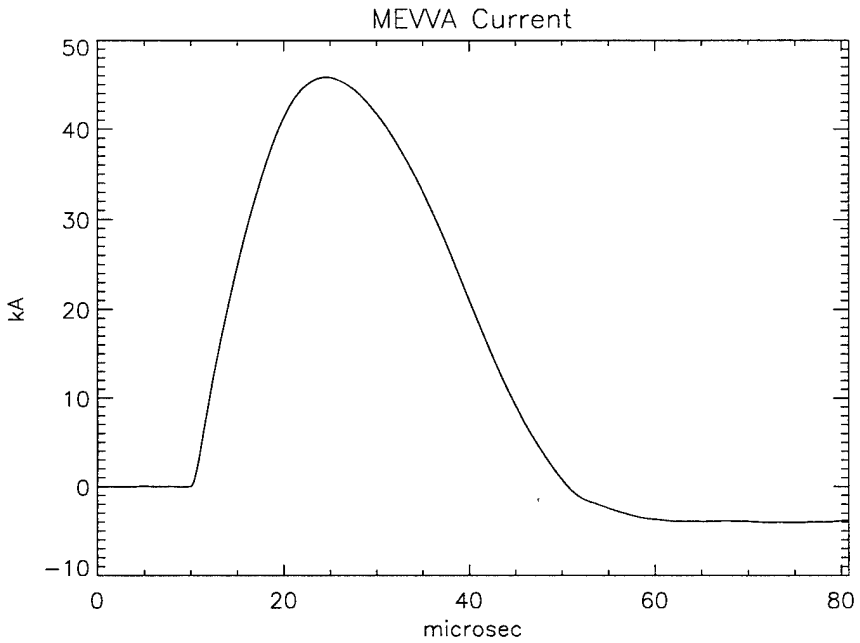

Figure 3-8. MEVVA current pulse at -1000 V charge with reduced inductance electrical feed.

Since very high current densities from the cathode are of interest, the cathode was reduced in size to 0.5″ from 0.75″. This reduction in area allowed an increase of approximately two in the current density at the cathode for the same overall current. The peak current density from the cathode is ~80 kA/cm^2. The apparatus has routinely been fired at this current density without serious damage to the cathode. The ~100 kA peak currents and ~80 kA/cm^2 current densities are the highest the MEVVA technology has achieved.

The change in the ground return path allowed several other changes to be made. In Figure 3-9 is shown the new vacuum electrical feed on Mark-I. With the closer connection to the anode, it was easier to make modifications to the anode geometry. A conical anode of stainless steel has been found to suffer little damage after multiple shots at currents of 100 kA. In addition, there is no change in the downstream current carried by the plasma when the tungsten mesh is attached to the end of the conical anode. The "downstream" current is defined here as the fraction of the diode current that flows beyond the end face of the conical anode (see Figure 3-9). This "leakage" current of the MEVVA is due to trapping of the magnetic field lines in the plasma as it blows downstream. This current is usually <3% of the total, and is measured by a downstream Rogowski coil. The capability of this anode design to operate without a mesh is an improvement at high current densities where a high transparency mesh is easily destroyed.

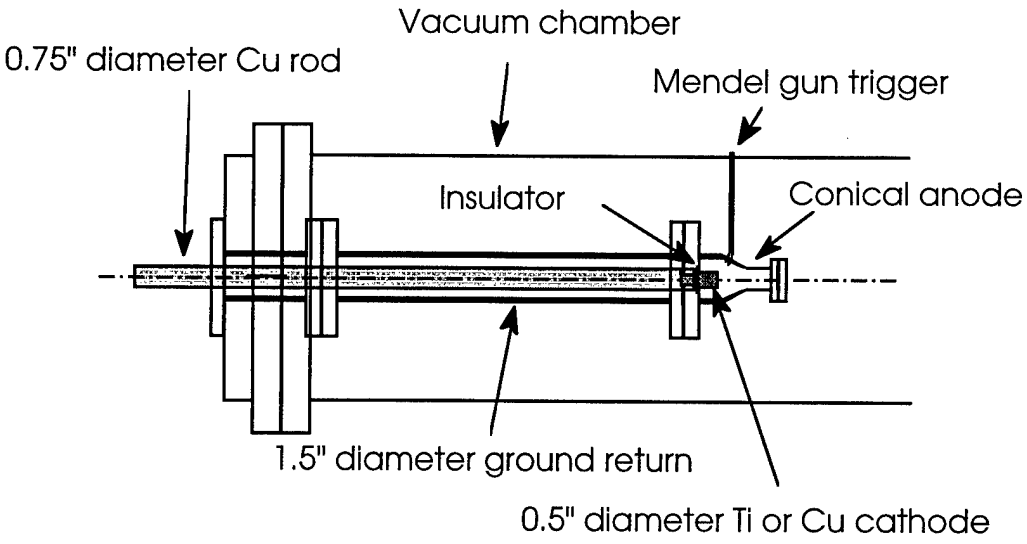

Figure 3-9. Schematic of the vacuum electrical feed for the MEVVA.

The diagnostic used to determine the ion density through most of this work was a biased, double Langmuir probe. Shown in Figure 3-10 is a schematic of the double probe circuit, and a drawing of the probe tips. The floating double probe circuit shown has two main advantages. It is not necessary to be electrically connected to the "noisy" ground, and the applied bias between the probe tips is independent of the plasma potential. The independence of the bias from the floating potential is particularly an advantage in MEVVA plasmas where the floating potential can be several tens of volts, which is on the same order as the applied voltage necessary to collect the ion saturation current from which the ion density can be inferred. Application of a voltage large enough to make the floating potential no longer important, forces the probe into a voltage regime where emission from the probe tip can mask the collected ion current signal. For the double probe, knowledge of the effective collecting area of the probe is essential to determine the density. The effect of the magnetic field, and of particle sheaths are important in

determining this effective collecting area.[4] The metal plasma created by the MEVVA can coat insulators and increase the collecting area of a probe if the conducting tip is in contact with the coated insulator. To avoid this problem, the collecting tip must be designed so that its point of contact with the insulator is shielded from the plasma. However this type of design can cause difficulties in determining the effective probe areas. By varying the probe geometries and areas, the effective collecting areas of the probes can be determined.

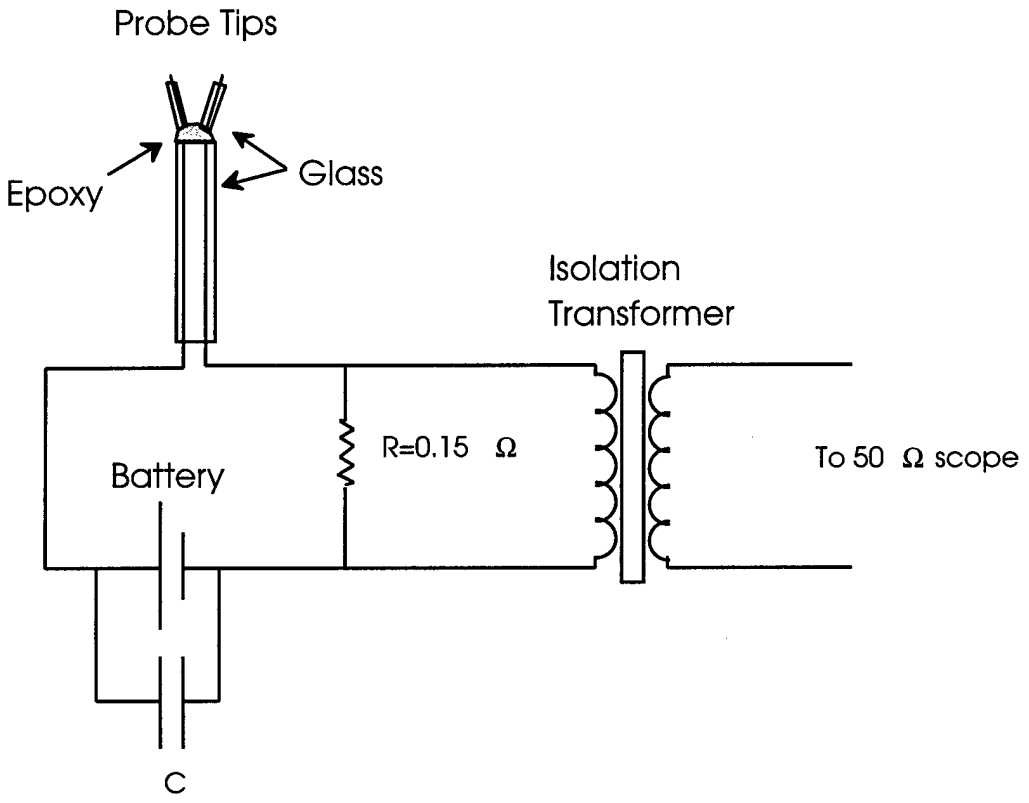

Figure 3-10. Double Langmuir probe circuit and probe tip geometry.

Data of the calculated ion density from probes of different collecting areas at approximately the same location in the plasma are shown in Figure 3-11. These data are from a discharge at -1000 V charge. Probe 1 has a much smaller area than probe 2, and hence is more susceptible to spatial variations in the plasma density, which explains why it shows more variation than probe 2. Possible errors in the assumed collecting areas, and possible saturation of the bias circuitry limit the accuracy of these measurements. However, these data demonstrate that the plasma density is in the appropriate range for use as an imploding load.

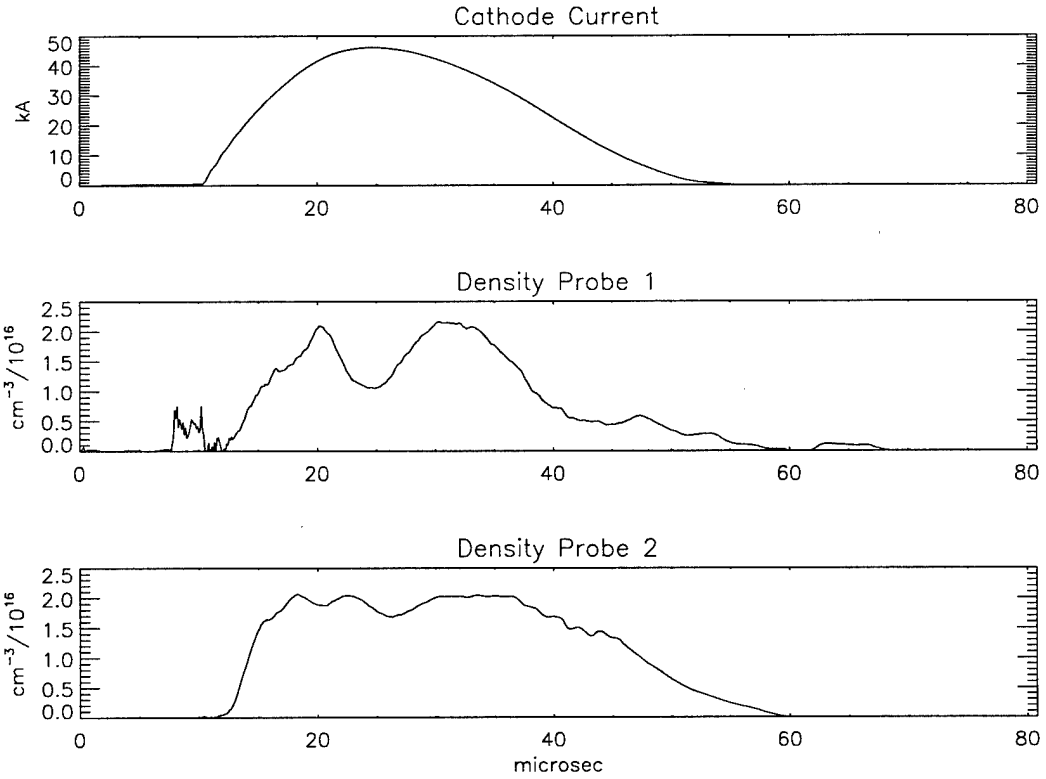

Figure 3-11. MEVVA current, and the ion density as calculated from two double Langmuir probes of different areas.

As an example of the density desired for an imploding load, the plasma ion density required for large radius implosions on SATURN is estimated as follows:

Assume a Ti load with a 5 cm outer diameter and a inner diameter of 1 cm on SATURN. The simplest mass estimate would come from the simple MR^2 scaling and would assume that the implosion time would be the same as for the optimum Al array (330 μg/cm at R=0.86 cm). The effective average radius (rms) for this proposed Ti load is ≈1.8 cm, and so the predicted optimum Ti mass ≈75 μg/cm. The average ion density would therefore be $n_i \approx 5\times10^{16}$ cm^{-3}. With a 1.8 cm diameter implosion, the average kinetic energy of the Ti ions should be approximately 4.4 times that of the optimum Al array. If the Al ions are assumed to have ≈15 keV/ion at implosion (h≈1.0), then the Ti ions should have ≈66 keV/ion. This is near the E_{min}= 83.4 keV/ion estimated by Whitney et al[5] and may produce efficient Ti k-shell emission. To increase the value of h, larger diameter shells might be needed. In that case, the plasma density required would be lower than the value of 5×10^{16} cm^{-3} estimated above.

To scale to the density that is necessary for SATURN, SRL has assumed that the ion density varies linearly with the MEVVA current. It has been found by numerous researchers[(6-9)] that the erosion rate of material from a MEVVA cathode is dependent upon the coulombs per second flowing through the cathode, not the voltage at the cathode. The data in Figure 3-11 were measured at a MEVVA voltage of -1000 V. To check the dependence of the ion density with cathode current, the peak measured ion density from a double probe is plotted versus cathode current density in Figure 3-12. The

double probe used is the probe labeled probe 2 in Figure 3-11. The data in Figure 3-12 clearly show a linear dependence of the ion density on the current density. Measured ion densities at higher cathode current densities than those shown in Figure 3-12 were not reliable due to the inability of the probe circuitry shown in Figure 3-10 to deliver adequate current.

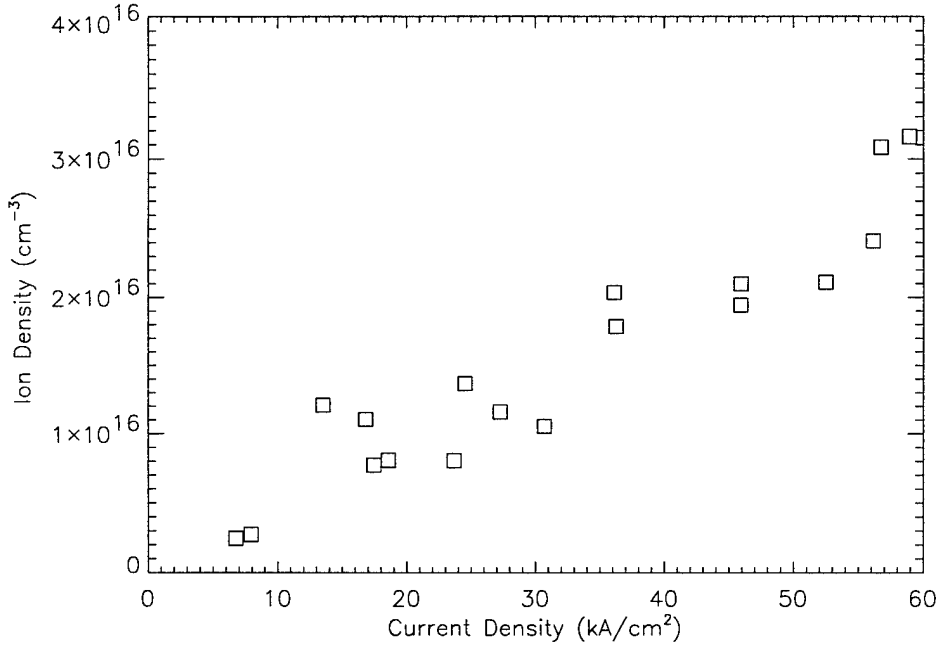

Figure 3-12. Peak measured ion density from the double probe as a function of cathode current density.

The Mark-I hardware, has surpassed both the previous highest current as well as current density drawn from a MEVVA. No practical limit on the current density has been found, or appears to exist. The argument that the plasma is formed in "hot spots" of high current density on the cathode, and that the total current is just the sum of these spots, is in agreement with what has been found. The absolute limit of the current density would

be the maximum packing fraction of these hot spots. However, the practical limits of inductance and resistance imply that to approach that limit, the energy deposited in the cathode from the rising current would be more than the cathode could sustain. In a nut shell, the practical limit on the current density is one of the energy deposited in the cathode, and not the instantaneous current density.

Before the operation of the low-inductance Mark-I MEVVA, it was unknown whether the plasma production during a short pulse (~50 μs) would be as high as in the standard long pulse (~10 ms) MEVVA discharges. Mark-I has found that the pulse length has not been a problem at all. It appears that with appropriate triggering, the onset of the plasma production is much faster than ~5 μs. Concerns that a long pulse is necessary to set up the high density plasma appear to be unfounded. This is advantageous for the Mark-II design, because only a flat top portion of the current pulse less than 10 μs long is necessary to fill the diode of a simulator. A pulse much longer than this requirement inefficiently uses the stored energy.

The density measurements presented so far have been made with double Langmuir probes, and agree well with predictions. However, there is always some question as to the accuracy of probe measurements, especially in the presence of a supersonic plasma, such as the MEVVA. When dealing with such density measurements, two independent diagnostics are desirable, and non-perturbing measurements are generally preferred. Due to concern expressed over the density measurements, SRL agreed to confirm the probe measurements with a laser interferometer. The interferometer was designed and

breadboarded by Dr. Stephen Fulgham and built in San Leandro to his design by Dr. Greene. These additional measurements were not planned in the original schedule.

Shown in Figure 3-13 is a schematic of the interferometer. The interferometer is a Mach-Zehnder type. The laser is a Melles Griot polarized HeNe laser with a minimum output of 2 mW at 632.8 nm. The output of the laser is slowly focused to a beam waist at the center of the probed plasma. The beams are then allowed to expand so that the image on the photodiodes is a magnified image of the beam waist. The magnified image reduces the effects of refraction of the probe beam due to density gradients. The beamsplitters are polarizing beamsplitters, oriented at 45 degrees to the polarization of the laser. In this orientation, the probe and reference beams are equal power beams, and any phase shift of the probe beam due to the electron density of the plasma causes a rotation of the polarization of the recombined beam. A second pair of beamsplitters oriented at 45 degrees to the first pair, splits the recombined beam into beams polarized parallel and perpendicular to the initial laser polarization. These final two beams are measured by EG&G FFD-200 fast photodiodes. Rotation of the polarization of the recombined beam increases the power in one of the final beams, while decreasing the power in the other. The two photodiodes are connected in a differencing bridge arrangement. Adjustment of the DC voltage applied to the PZT varies the relative phases of the probe and reference beams. A low-pass, active feedback circuit on the PZT can be used to balance the laser power into the photodiodes. In this design, the baseline signal is zero at the interferometer's point of maximum sensitivity, which allows for the possibility to measure phase shifts as small as 10^{-5} of a wave.

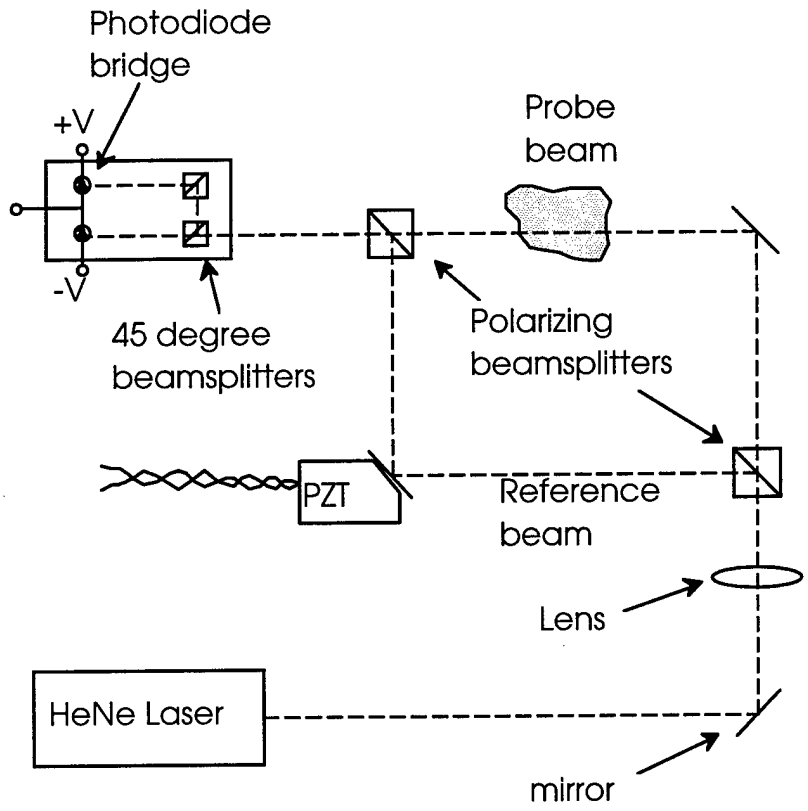

Figure 3-13. Schematic of HeNe laser interferometer.

In Figure 3-14, traces of a typical discharge with the raw interferometer trace, as well as the inferred line integrated density are shown. The large spikes seen on the traces during the rise of the current is noise due to the trigger circuit. A voltage is applied to the PZT after the discharge to sweep the interferometer through a full wave to find the values of the peaks. To calculate the density, the radial location of the interferometer is scanned over several shots, and an Abel inversion applied to the resultant data.

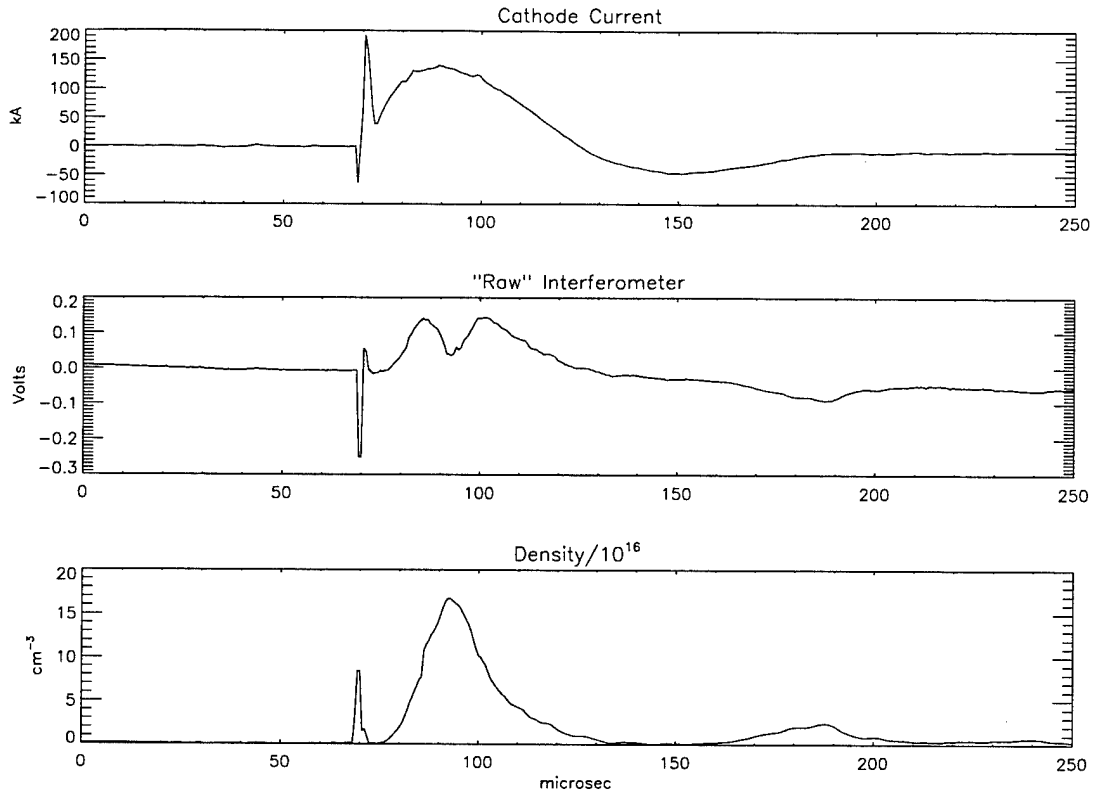

Figure 3-14. Typical discharge with the raw interferometer signal and the calculated line integrated electron density.

As the ion density is increased, it is expected that the ability of the magnetic field to confine the plasma will be reduced. In an effort to increase the amount of plasma delivered to the simulator AK gap without bringing the MPS too close to the gap to survive, an extended anode design was implemented on Mark-I. The change is basically an axial extension of the small diameter end of the anode cone. The ID of 2 cm of the extension matches the ID of the last portion of the cone. It was hoped that the stainless steel extension would greatly aid the confinement of the plasma without the usual problems of losses to the walls. Extensions of 7.5 cm and 20 cm were tested. These

lengths were chosen because they put the ends of the anode extensions at the edges of windows for diagnostic access. Line integrated electron density measurements were made across a chord which passed through the center of the plasma. With the 7.5 cm extension, the highest line integrated electron densities yet measured on Mark-I were found. The line integrated electron density with the 20 cm extension was approximately 75% of the value with the 7.5 cm extension. The 25% drop in measured density with the longer extension is approximately equal to the drop measured at that location without the anode extension. However, the radial extent of the plasma is much reduced with the extension, so the extension has been found to be extremely beneficial for plasma confinement, without appearing to have increased losses. The use of a similar anode arrangement on the simulator, will allow the MPS to deliver the desired mass to the AK gap, and have the more expensive, more difficult to replace hardware a sufficient distance from the pinch to survive multiple shots. The anode extension becomes a reasonably inexpensive replaceable component. The solid anode extension also guarantees that there is no diffusion of plasma into the main chamber where it may then drift into the MITL. Past the end of the extension the plasma is free to expand, and the spatial distribution of this plasma is critical for the MPS.

Shown in Figure 3-15 is a surface plot of the line integrated electron density approximately 2.5 cm from the end of the 7.5 cm anode extension. The line integrated density is plotted as a function of time and radial location. In Figure 3-16, an Abel inversion is performed on the data, and the calculated density as a function of time and radial location is shown.

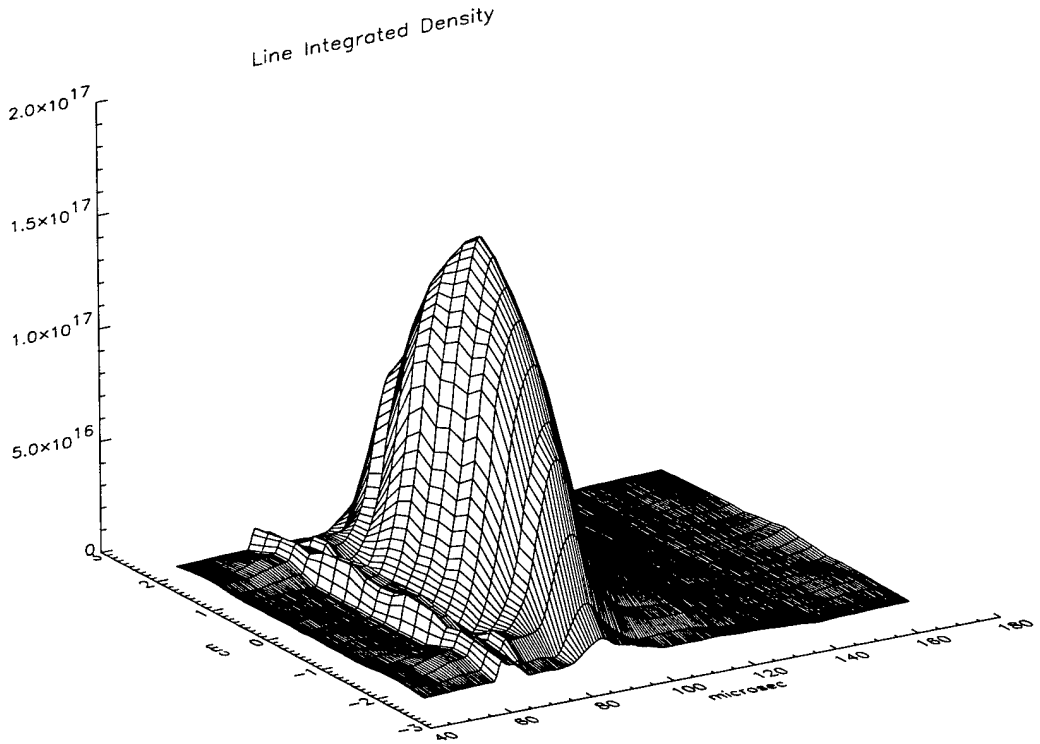

Figure 3-15. Surface plot of the line integrated electron density as a function of time and radial location 2.5 cm from the anode.

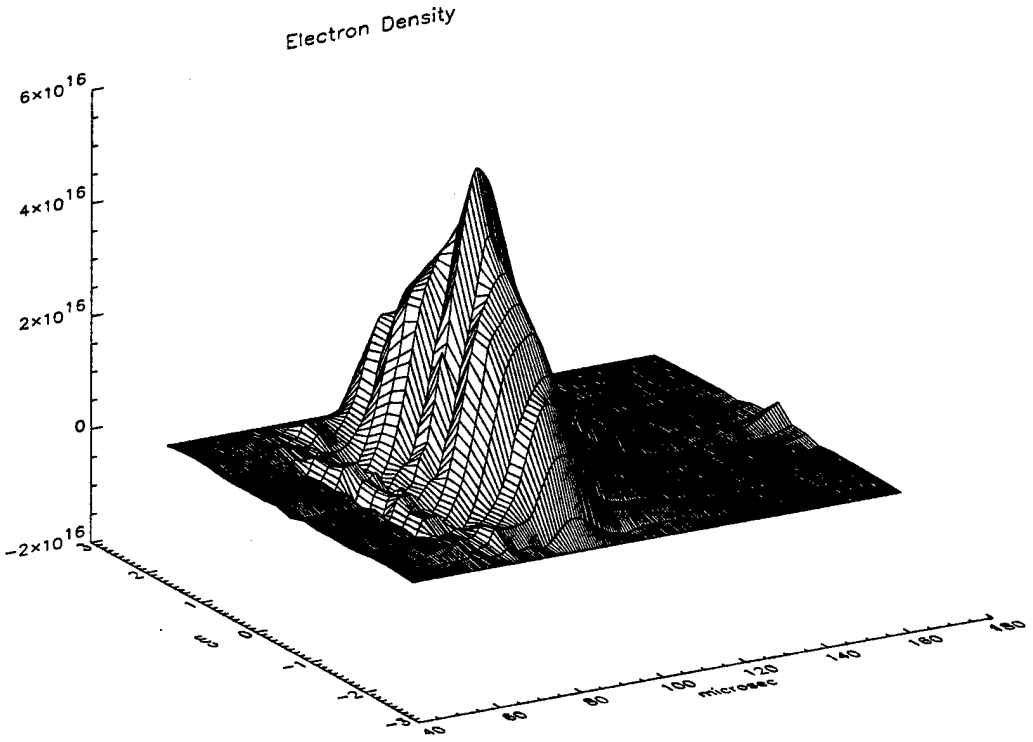

Figure 3-16. Surface plot of the calculated electron density as a function of time and radial location. These data are calculated from an Abel inversion of the data in Figure 3-15a.

The data in Figure 3-16 show electron densities comparable to those previously inferred from the double probe signals. For a Ti plasma with a temperature of 4-8 eV, the average ionization state is probably Z~2-4. Although these densities are very encouraging, and appear to say that this source can deliver the mass density desired, the distribution is broader than what would be expected. Recall that the interferometer is only 2.5 cm from the end of the 2 cm ID anode extension, and note that the width of the region of the plasma above a density of 10^{16} cm^{-3} is ~4 cm. To examine this expansion, which is

more rapid than expected, visible light images were taken of the plasma at the exit of the 7.5 cm anode extension (Figure 3-17). Figure 3-16 shows a plasma from ~120 kA peak current discharge in a ~4 kG axial magnetic field expanding rapidly away from the end of the anode. This image implies that the cross field diffusion of the plasma at these densities and magnetic field levels is a serious concern, and the scaling of the cross field diffusion is important.

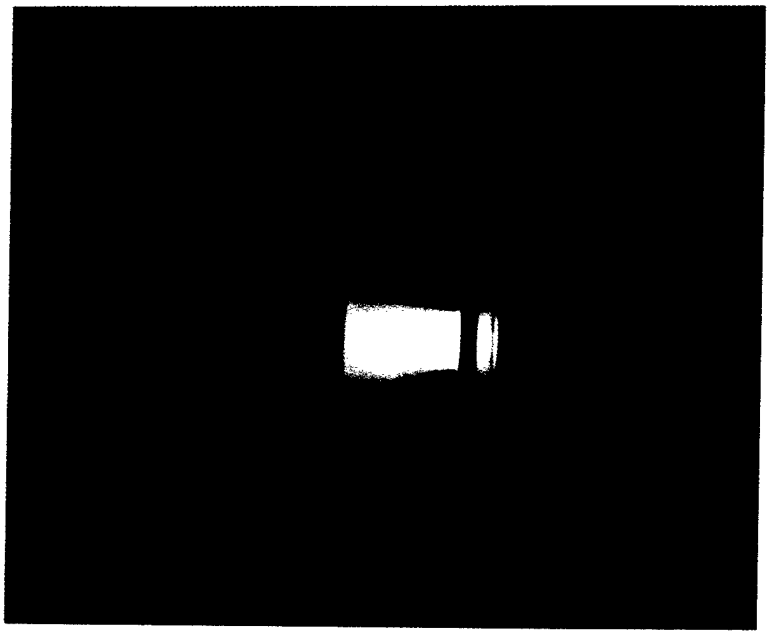

Figure 3-17. Visible light emission from the plasma at the anode exit with ~4 kG of axial magnetic field.

The MEVVA source has been studied for many years as a plasma centrifuge for isotope separation.[10,11] The separation of the isotopes is dependent upon the cross field diffusion of the ions. For the densities and temperatures typical for the centrifuge, it can be shown that the diffusion rate is likely to be defined by Bohm like diffusion rather than classical diffusion. The basic principle by which the centrifuge works is that a self-

consistent, radial electric field develops across the plasma, perpendicular to the applied magnetic field. The E×B drift which ensues corresponds to a rotation of the plasma. The E×B rotation drives the diffusion across the magnetic field. It can be shown that diffusion driven by the E×B rotation scales like Bohm diffusion, which has been found to accurately predict the diffusion rates for many types of plasmas.[12] The Bohm diffusion coefficient is,

$$D \approx \alpha \frac{kT}{eB}$$

where the scale factor α is set equal to 1/16. This diffusion coefficient is independent of the plasma density. The independence of this diffusion on the density, and the data in Figure 3-6, had implied that the cross field diffusion would not be of concern at the desired densities. However, the classical diffusion coefficient calculated from the effects of non-like particle collisions predicts diffusion dependent upon the density. The classical diffusion coefficient is

$$D = \frac{2n\eta kT}{B^2} \quad ,$$

where n is the density and η is the perpendicular resistivity of the plasma.[12] Classical diffusion is typically much less than Bohm diffusion due to its dependence upon the square of the magnetic field, and usually it can be ignored in comparison. However, for the high densities which the MEVVA source is now producing, the cross field diffusion may be determined by classical diffusion scaling rather than Bohm diffusion. At higher densities the particle collisions may become more important than the electric fields which cannot "propagate" as far in the higher density plasma which has a correspondingly smaller Debye

length. For the inferred densities, temperatures and scale lengths of the plasma shown in Figure 3-17, the classical diffusion coefficient is much larger than the Bohm. The calculated value implies that the plasma is free to expand at the sound speed, since the diffusion speed (v=D/scale length) is larger than the sound speed. This discovery was not encouraging for the project, but the image in Figure 3-17 shows better collimation than simple expansion of a sub-sonic gas into vacuum. This result should not be surprising as SRL has maintained that the plasma is at least *slightly* supersonic.

To confirm this assertion, an image of the plasma at the anode exit without axial magnetic field is shown in Figure 3-18. The image clearly shows better collimation of the plasma than would be expected for sub-sonic expansion of an ideal gas into vacuum. If it is super-sonic expansion into vacuum, the expansion angle is a function of the Mach number of the flow. The relationship between the Mach number and the expansion angle of supersonic flow into vacuum is

$$M = \sin\left(\frac{1}{\alpha}\right)$$

where M is the Mach number and a is the angle of expansion. The Mach number inferred from the expansion angle for this plasma is M≈4. This Mach number is comparable to the flows from standard gas puffs.

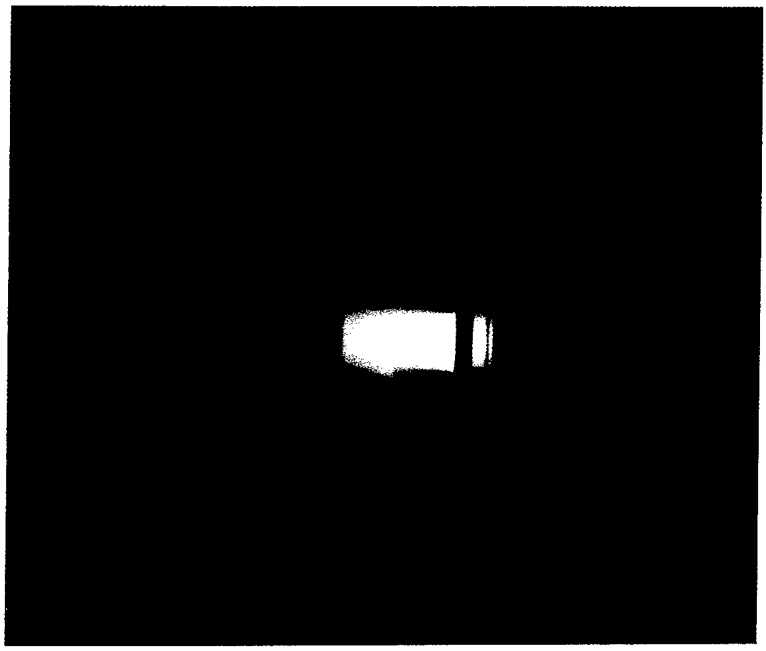

Figure 3-18. Visible light emission at end of anode without the axial magnetic field.

The visible light images corroborate well with the measured line integrated electron densities from the interferometer. In Figure 3-19 is shown the line integrated electron density at about 2.5 cm from the end of the anode extension, and in Figure 3-20 the calculated electron density is shown. The calculated density does not have appreciable extent beyond a diameter of 2 cm, which is in good agreement with the visible light images. By insulating regions of the anode from the MEVVA current, nearly all of plasma produced without a magnetic field can be made to exit the anode, and the line integrated density is equal to that with the magnetic field. This implies that the net plasma produced is approximately the same, but the more limited extent of the plasma implies a higher peak density. The density profile calculated is highly peaked on axis, and its peak value is higher than the peak calculated density with the applied field.

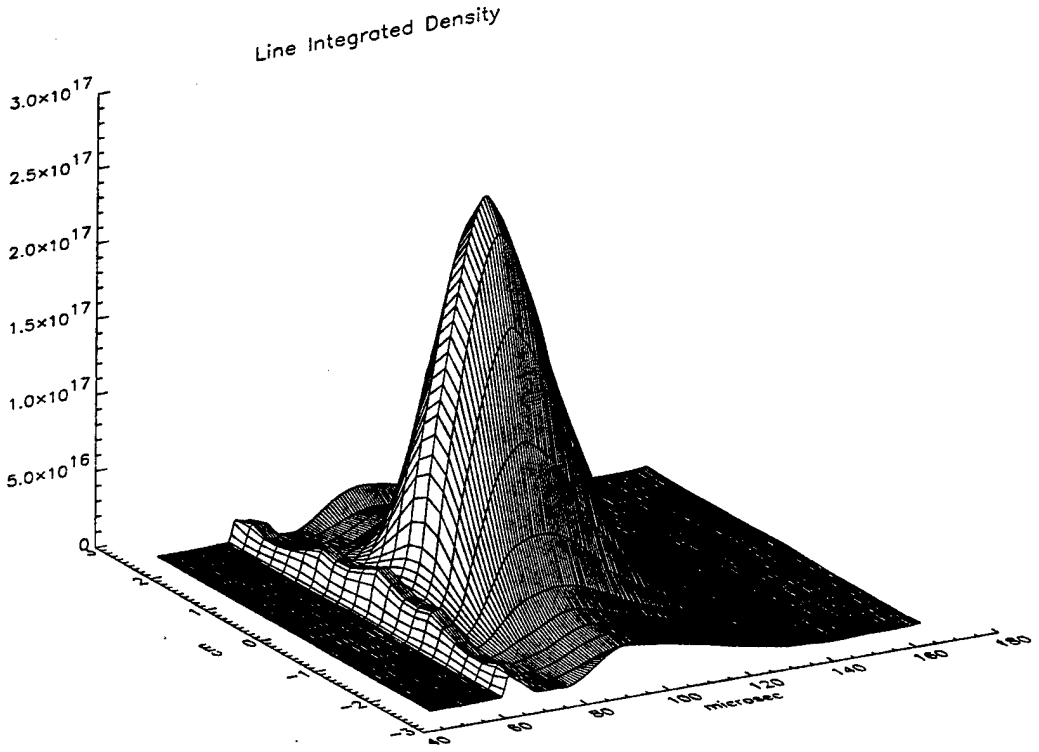

Figure 3-19. Surface plot of the line integrated electron density as a function of time and radial location 2.5 from the anode, without an applied magnetic field.

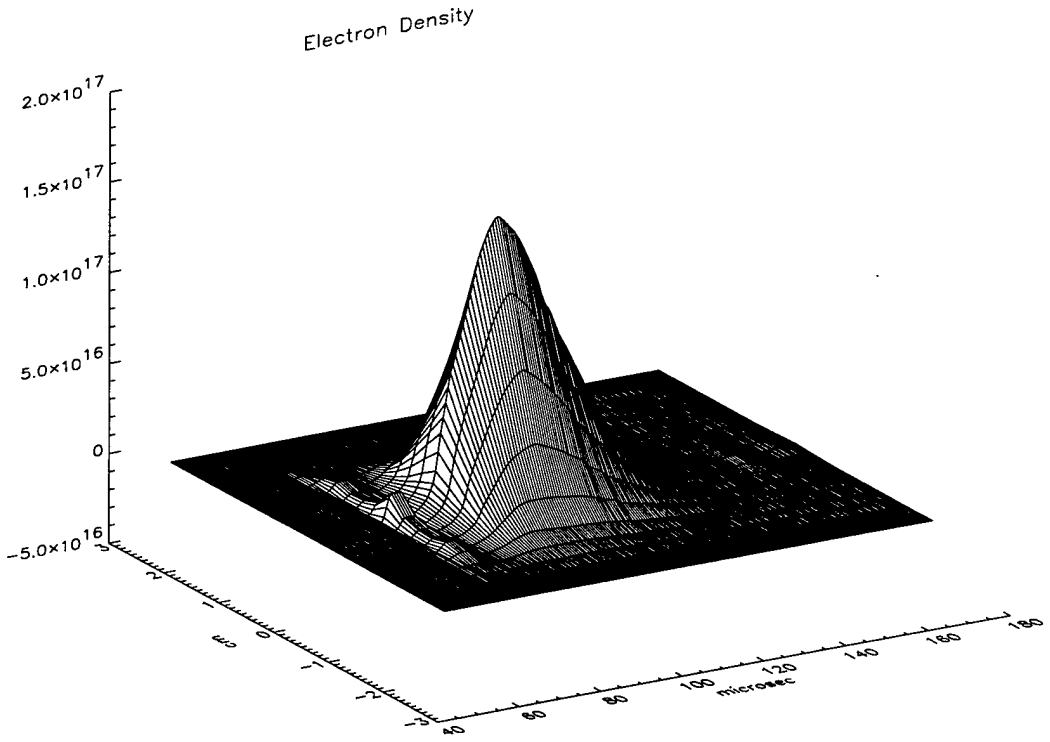

Figure 3-20. Surface plot of the calculated electron density as a function of time and radial location. These data are calculated from an Abel inversion of the data in Figure 3-19.

Both the visible light images and the electron densities from the interferometer in the non-magnetized case appear to show better collimation of the plasma than in the magnetized case. This difference is probably due to a difference in the nature of the arc in the anode-cathode gap when there is an applied magnetic field. The expected cross-field diffusion due to E×B rotation with the applied field, is not enough to account for the apparently more rapid expansion. (Recall that the previously calculated Bohm diffusion coefficient was much smaller than the classical.) In addition, the pictures show evidence

of a "halo" in the magnetized case which may imply a higher temperature, although probe measurements were unable to detect a difference in electron temperatures. It appears that with the applied magnetic field the source plasma is produced in a slightly broader peak, as evidenced by the interferometer data, with perhaps some difference in temperature. The difference may be due to a change in the current attachment with the field. This difference increases the radial expansion of the plasma relative to the strongly peaked on axis, non-magnetized case. This is not a problem for the source on a simulator because if a magnetic field is desired, it will be fairly straight forward to shield the anode-cathode gap from the applied field with highly conducting walls and/or high μ materials.

The MEVVA source, with its anode-cathode gap shielded from the magnetic field, should be better collimated than a Mach 4 gas puff, and be fully ionized, removing the need for pre-ionizing circuits. If it is felt that the magnetic field is limiting the compression ratio of the pinch, then the MPS can be operated without the magnetic field, and its radial collimation should still be adequate.

The Mark-I apparatus has enabled us to design a Mark-II apparatus which is capable of being fielded on a simulator with an adequate degree of confidence in its ability to deliver the required mass. In the next section the Mark-II design will be described.

3.2 MARK-II DESIGN.

To ensure that the delivered mass scales in the manner determined from Mark-I, the Mark-II hardware has been designed as close to multiple copies of the Mark-I apparatus as possible. The Mark-II design for implementation on a machine such as

Double Eagle or Phoenix consists of an array of 12 MPS diodes. The schematic drawings of the diode array is shown in Figures 3-21 and 3-22. The current feed to each diode is completely separate up to the cathode tip. This ensures the azimuthal uniformity of the source. Each cathode has its own capacitor bank, which is inductively isolated from the other banks, and each cathode is connected to the capacitor bank with two coaxial cables to the back of the diode array. The two cables parallel feed is necessary to keep the total inductance for each cathode down as low as possible to match the conditions of the Mark-I apparatus. The coaxial cables have a high current, "banana plug" type connection which allows for a quick, easy and reproducible method of making and breaking the electrical connections. Inside the diode array, the current is carried by pie-wedge shaped Cu conductors which join onto Cu extension pieces. The extension pieces can be easily replaced, to allow for changes in the radius of the cathode array. The cathode tips are connected to the extension pieces, and are made of the desired plasma material. For the design shown in Figures 3-21 and 3-22, the tips are made of titanium at a mean diameter of 3 cm.

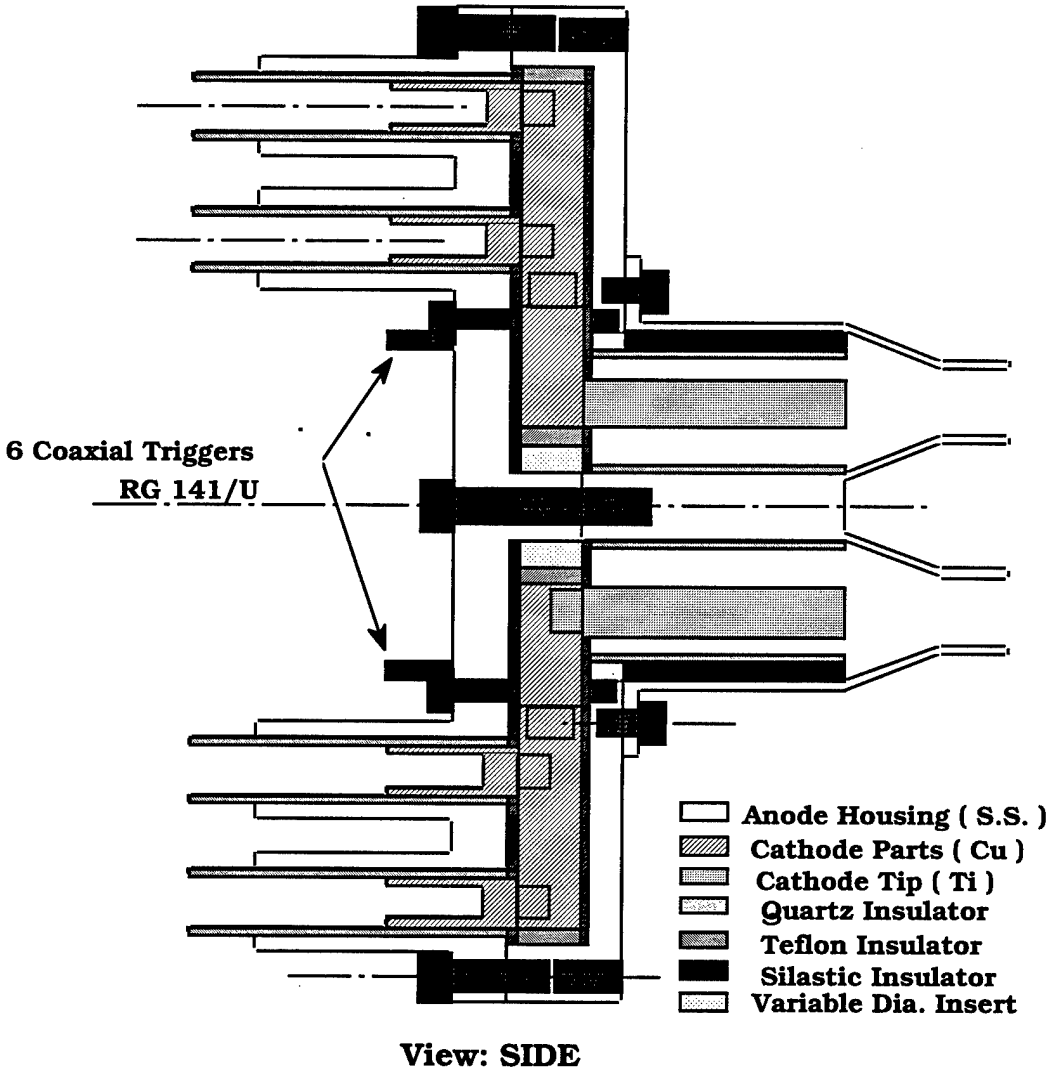

Figure 3-21. Cut-away side view of MPS annular diode array.

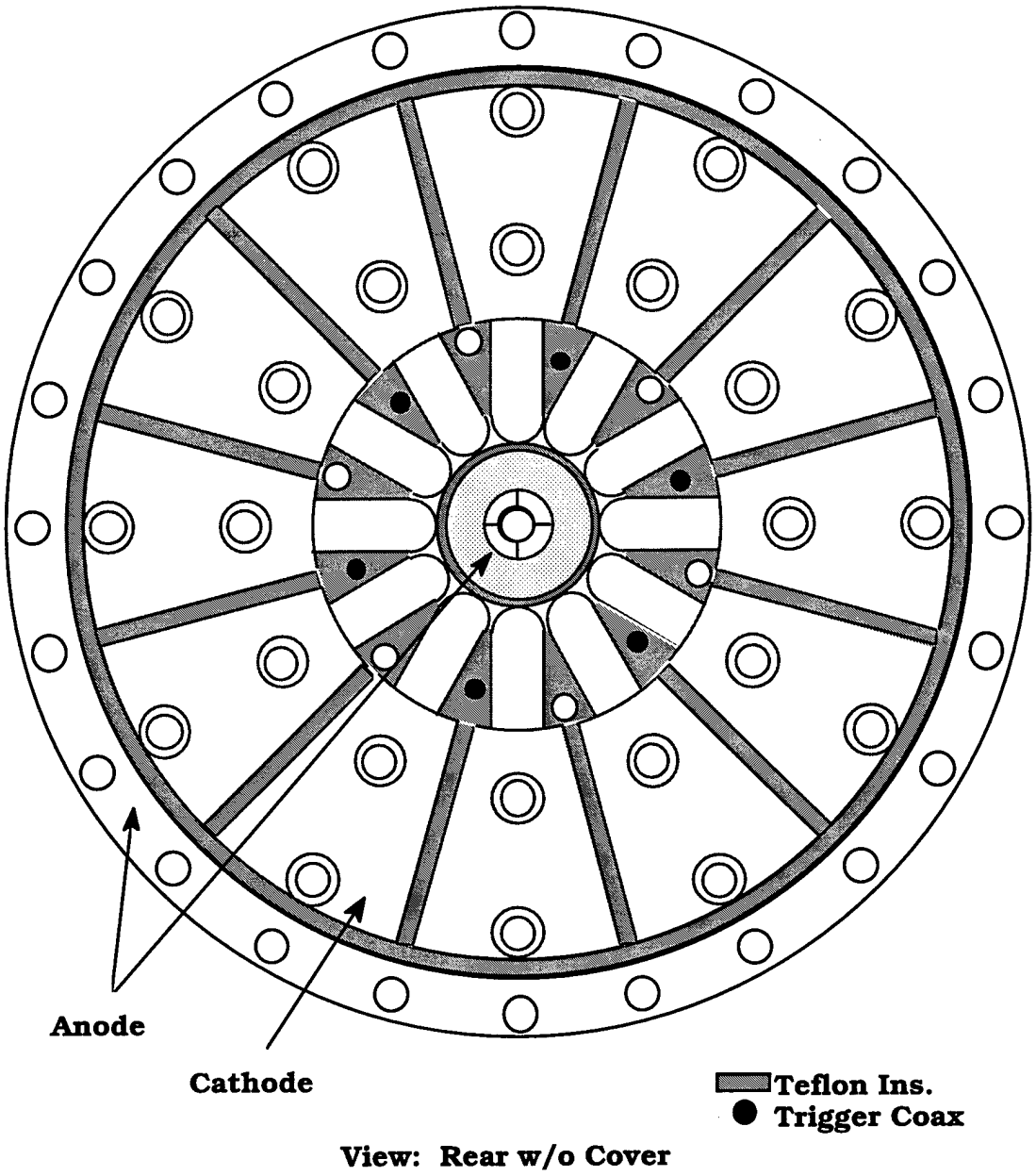

Figure 3-22. Cut-away rear view of MPS annular diode array.

The anode nozzle for the entire array of cathodes is made of two pieces, connected to make an annular ring for the nozzle opening. Although this makes the current return in

the anode nozzle communal, it will not affect the current from each individual cathode. The annular opening for the anode should increase the azimuthal uniformity of the source as it allows diffusion of the plasma between the individual diodes inside the anode, before entering the simulator pinch region.

The triggers for the diodes are fed in through the back of the diode array, and there is one trigger cable for every two cathodes. This number of trigger cables has been chosen to ensure that every cathode is adjacent to a trigger cable, although, in practice it is expected that it won't be necessary to have that many trigger cables. The small amount of plasma that is produced by the cable gun trigger reliably starts the MEVVA discharge within 1 μsec of the triggering time. The copious plasma produced by a single MEVVA should also trigger any adjacent MEVVA, which would make the longest possible delay between the firing of any two diodes approximately 6 μsec. That delay should still be acceptable, as there would be adequate overlap in the peak densities of the produced plasmas from the diodes. The multiple trigger locations should give even better coincidence of the peak densities of the produced plasmas.

To achieve density profiles that are appropriate for implosions on Double Eagle or Phoenix, the cathode tips in the diode array are to nominally be at a 3 cm mean diameter. This design is for the 5 cm OD, 1 cm ID annular load described earlier in this report. To be able to test other initial conditions, cathode extension pieces, and anode pieces for a larger and a smaller mean diameter are planned. The ability to change between three mean diameters, along with the ability of the MEVVA plasma to deliver varying densities allows a wide shot matrix to test the MPS.

The configuration for implementing the MPS on a simulator is shown in Figure 3-23. The MPS is fired into the AK gap of the simulator, which has a small "get-lost" region for the MPS plasma. The get-lost region is to reduce the risk of the plasma shorting out the MITL. Since the rise-time of the MPS is much faster than a typical gas puff, and the metal plasma tends to stick to metallic surfaces, the risk due to firing into the gap is much less with the MPS than it would be with the standard gas puff.

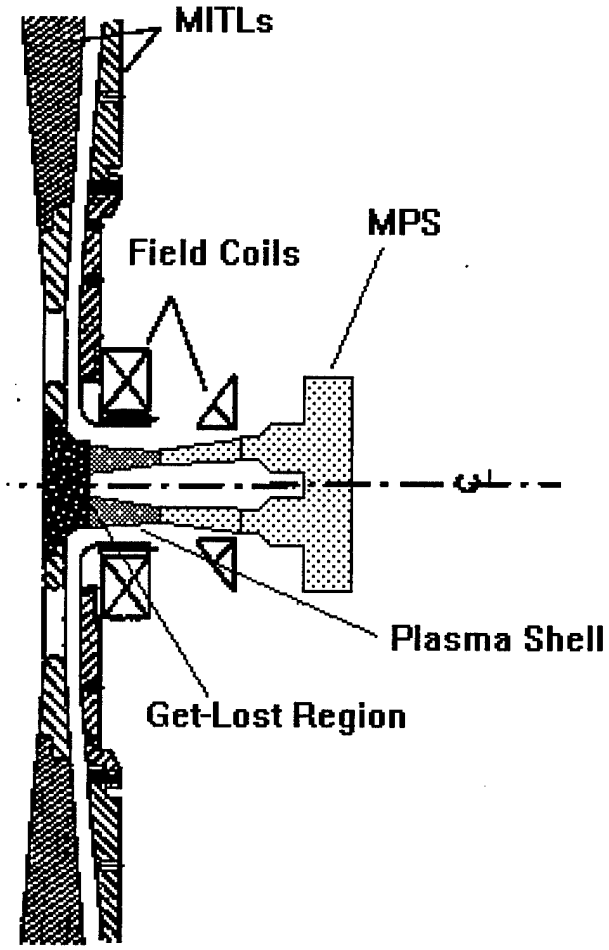

Figure 3-23. Configuration of the MPS firing into the simulator AK gap.

SECTION 4

SUMMARY OF TASK 3.3

The design of the nested shell implosion is a combination of the MPS described above, and the gas puff design shown in Figure 2-1. An MPS source of a small diameter is fired into a larger diameter gas puff of CH_4 or other low-Z gas. The gas puff is located in the get lost region shown in Figure 3-23, and has a small get-lost region on axis to accommodate the inner plasma shell. The gas puff is more azimuthally uniform than a wire array of carbon fibers, and this design should implode better than the original nested shell tests discussed earlier.

SECTION 5

CONCLUSIONS

Under this contract SRL has achieved net currents, current densities, and plasma densities much higher than those previously reported. The capabilities of the MEVVA technology to produce extremely high density plasmas with spatial distributions appropriate for use as an imploding load on a high current z-pinch has been demonstrated. Peak electron densities of ~1.5×10^{17} cm^{-3} and average electron densities of ~5×10^{16} cm^{-3} over usable spatial distributions have been measured. The MEVVA source has been shown to be able to operate both with and without a magnetic field with adequate radial collimation, and the delivered density can easily and accurately be adjusted over a wide range with simple voltage programming of the source. The Mark-II design allows for multiple source radii and spatial distributions to give a broad possible shot matrix for optimization of the source. The measured parameters of the MPS show it to be appropriate for implementation on a simulator of the scale of Double Eagle or PHOENIX, and after validation on a driver of that size, implementation on SATURN could be considered.

SECTION 6

REFERENCES

1. J.L Giuliani et al. "Numerical Simulations of PRS Yields for a Pulsed Power DECADE Class Generator (U)", Journal of Radiatin Effects, Research and Engineering, Vol 12, Number 3, September 1994, p. 41. (UNCLASSIFIED)

2. Science Research Laboratory draft final technical report entitled "Higher Efficiency X-Ray Load Designs For Z-Pinch Implosions (U)", dated June 9, 1992. (UNCLASSIFIED)

3. J. Watrous and M. Frese, "Applied Field Confinement of Vacuum-Arc-Generated Metal Plasma (U)", Draft Final Report 93-08, NumerEx, (1993). (UNCLASSIFIED)

4. I.H. Hutchinson, "Principles of Plasma Diagnostics (U)", Cambridge University Press, New York, (1987) pp. 50-75. (UNCLASSIFIED)

5. K.G. Whitney et al., "Advanced Concepts Theory Annual Report 1992, Final Report (U)", NRL/MR/6722--93-7301, p. 3. (UNCLASSIFIED)

6. R. Prasad, R. Consiglio and, M. Krishnan, IEEE Trans, on Plasma Sci. (U), PS-14 (1986), p.498. (UNCLASSIFIED)

7. A. Plyutto, V. Ryzhov, and A. Kapin, Sov. Phys. JETP (U), vol. 20, (1965), pp 328-337. (UNCLASSIFIED)

8. C. Kimblin, J. Appl. Phys., vol. 44 (U), (1973) pp. 3074-3081. (UNCLASSIFIED)

9. A. Nürnberg, D. Fang, U. Bauder, R. Behrisch, F. Brossa, J. Nucl. Mat., 103&104 (U), (1981), p.305. (UNCLASSIFIED)

10. R. Prasad, Ph.D. thesis (U), Yale University, (1986). (UNCLASSIFIED)

11 R. Prasad and M. Krishnan, J. Appl. Phys., **61** (U), (1987), p.4464. (UNCLASSIFIED)

12. F. Chen, "Introduction to Plasma Physics and Controlled Fusion, Volume 1: Plasma Physics (U)", Plenum Press, New York, (1984). (UNCLASSIFIED)

DISTRIBUTION LIST

DSWA-TR-95-88

DEPARTMENT OF DEFENSE

DEFENSE INTELLIGENCE AGENCY
ATTN: DIW-4

DEFENSE SPECIAL WEAPONS AGENCY
ATTN: GERDING
ATTN: JOAN MA PIERRE
2 CY ATTN: ESA
ATTN: DR G DAVIS
ATTN: W SUMMA
ATTN: ESE
ATTN: R C WEBB
ATTN: W J SCOTT
ATTN: L PRESSLEY
2 CY ATTN: ISST
ATTN: PMPO
ATTN: P HEBERT
ATTN: MAJ K ZERINGUE
ATTN: TDSP
ATTN: WEL
ATTN: T HOOVER
ATTN: LTCOL KYME

DEFENSE TECHNICAL INFORMATION CENTER
2 CY ATTN: DTIC/OCP

FIELD COMMAND DEFENSE SPECIAL WEAPONS AGENCY
ATTN: FCTI
ATTN: R W SHOUP
ATTN: DR BALADI

DEPARTMENT OF THE ARMY

ARMY RESEARCH LABORATORIES
ATTN: TECH LIB
ATTN: G HUTTLIN

MISSILE DEFENSE & SPACE TECHNOLOGY CTR
ATTN: R CROWSON

U S ARMY CORPS OF ENGINEERS
ATTN: DR LEVERENZ

U S ARMY TRADOC ANALYSIS CTR
ATTN: ATRC-WSS-R

USASSDC
ATTN: I MERRITT
ATTN: G POLLOCK
ATTN: D BRADSHAW

DEPARTMENT OF THE NAVY

NAVAL RESEARCH LABORATORY
ATTN: DR C D BOND
ATTN: J SETHIAN
ATTN: D MOSHER
ATTN: G COOPERSTEIN
ATTN: R COMMISSO

SPACE & NAVAL WARFARE
ATTN: LCDR J SMITH
ATTN: R WOODS

DEPARTMENT OF THE AIR FORCE

PHILLIPS LABORATORY
ATTN: D H HILLAND

SAN ANTONIO AIR LOGISTICS CTR
ATTN: F CRISTADORO

SPACE SYSTEM DIVISION/XR
ATTN: SMC/CC
ATTN: SMC/CNJZ
ATTN: SMC/CZEA
ATTN: SMC/EN
ATTN: SMC/MBSS
ATTN: SMC/MGS
ATTN: SMC/XRX

SSP-27334 TRIDENT
ATTN: J BURTLE
ATTN: K TOBIN

USAF/AEDC/DOT
ATTN: CAPT FRANK FAIRCHILD

DEPARTMENT OF ENERGY

LAWRENCE LIVERMORE NATIONAL LAB
ATTN: J NUCKOLLS

LOS ALAMOS NATIONAL LABORATORY
ATTN: J BROWNELL

SANDIA NATIONAL LABORATORIES
ATTN: L D POSEY
ATTN: M HEDEMANN
ATTN: M K MATZEN
ATTN: MARTIN FUNTES
ATTN: D COOK
ATTN: R E PEPPING
ATTN: TECH LIB
ATTN: W BALLARD
ATTN: W BEEZHOLD

U.S. DEPARTMENT OF ENERGY
OFFICE OF MILITARY APPLICATIONS
ATTN: C B HILLAND

OTHER GOVERNMENT

CENTRAL INTELLIGENCE AGENCY
ATTN: J PINA

DEPARTMENT OF DEFENSE CONTRACTORS

ADVANCED RESEARCH AND APPLICATIONS CORP
ATTN: R ARMISTEAD

ALME AND ASSOCIATES
ATTN: JOHN F DAVIS
ATTN: S SEILER

ALME AND ASSOCIATES
ATTN: JOHN F DAVIS
ATTN: S SEILER

APTEK INC
ATTN: T MEAGHER

BDM FEDERAL INC
ATTN: W BETOWT
ATTN: W LARRY JOHNSON

CALSPAN CORP/AEDC
ATTN: C JETT
ATTN: L S CHRISTENSEN

DEFENSE GROUP INC
ATTN: ROBERT POLL

HUGHES AIRCRAFT COMPANY
ATTN: SCG-S41

JAYCOR
ATTN: J R MILLARD
ATTN: T FLANAGAN

JAYCOR
ATTN: CYRUS P KNOWLES
ATTN: R SULLIVAN

JAYCOR
ATTN: C ROGERS
ATTN: S ROGERS

KAMAN SCIENCES CORP
ATTN: D CALDWELL
ATTN: D JANSEN

KAMAN SCIENCES CORP
ATTN: CLAUDE FORE
ATTN: E DRISCOLL

KAMAN SCIENCES CORPORATION
ATTN: DASIAC

LOGICON R AND D ASSOCIATES
ATTN: B WEBSTER

MAXWELL LABORATORIES INC
ATTN: DR JASON WILKENFELD

MAXWELL LABS
ATTN: DR G GURTMAN
ATTN: WILLIAM H RIX

MAXWELL TECHNOLOGIES INC
ATTN: E WAISMAN
ATTN: N LOTER

MISSION RESEARCH CORP
ATTN: J R HENLEY

PHYSICS INTERNATIONAL CO
ATTN: C STALLINGS
ATTN: J GOYER
ATTN: J RIORDAN
ATTN: S L WONG

PULSE SCIENCES INC
ATTN: I D SMITH
ATTN: P W SPENCE

SCIENCE APPLICATIONS INTL CORP
ATTN: W CHADSEY

SCIENCE RESEARCH LAB
2 CY ATTN: P GREENE

THE AEROPSACE CORP
ATTN: M HOPKINS

THE AEROSPACE CORP
ATTN: LIBRARY ACQUISITION
ATTN: T PARK

W J SCHAFER ASSOCIATES INC
ATTN: E ALCARAZ